

# *Mechanisms producing different precipitation patterns over north-eastern Italy: insights from HyMeX-SOP1 and previous events*

Article

Accepted Version

Davolio, S., Volonté, A., Manzato, A., Pucillo, A., Cicogna, A. and Ferrario, M.E. (2016) Mechanisms producing different precipitation patterns over north-eastern Italy: insights from HyMeX-SOP1 and previous events. *Quarterly Journal of the Royal Meteorological Society*, 142 (S1). pp. 188-205. ISSN 1477-870X doi: <https://doi.org/10.1002/qj.2731> Available at <https://centaur.reading.ac.uk/88726/>

It is advisable to refer to the publisher's version if you intend to cite from the work. See [Guidance on citing](#).

To link to this article DOI: <http://dx.doi.org/10.1002/qj.2731>

Publisher: Royal Meteorological Society

All outputs in CentAUR are protected by Intellectual Property Rights law, including copyright law. Copyright and IPR is retained by the creators or other copyright holders. Terms and conditions for use of this material are defined in the [End User Agreement](#).

[www.reading.ac.uk/centaur](http://www.reading.ac.uk/centaur)

## **CentAUR**

Central Archive at the University of Reading

Reading's research outputs online



**Mechanisms producing different precipitation patterns over North-Eastern Italy: insights from HyMeX-SOP1 and previous events**

Journal:	<i>QJRMS</i>
Manuscript ID	QJ-15-0126.R2
Wiley - Manuscript type:	HyMeX Special Issue
Date Submitted by the Author:	n/a
Complete List of Authors:	Davolio, Silvio; Institute of Atmospheric Sciences and Climate (ISAC), National Research Council of Italy (CNR) Volontè, Ambrogio; University of Reading, Department of Meteorology Manzato, Agostino; ARPA FVG - OSMER, Pucillo, Arturo; ARPA FVG - OSMER, Cicogna, Andrea; ARPA FVG - OSMER, Ferrario, Massimo; ARPA Veneto,
Keywords:	heavy precipitation, orography, convection, HyMeX, Alps

**Mechanisms producing different precipitation patterns over North-Eastern Italy: insights from HyMeX-SOP1 and previous events**

S. Davolio<sup>a,\*</sup>, A. Volonté<sup>b</sup>, A. Manzato<sup>c</sup>, A. Pucillo<sup>c</sup>, A. Cicogna<sup>c</sup>, M. E. Ferrario<sup>d</sup>

<sup>a</sup>Institute of Atmospheric Sciences and Climate (ISAC), National Research Council of Italy (CNR), Bologna, Italy

<sup>b</sup>Department of Meteorology, University of Reading, UK – formerly Dep. of Physics, University of Milan, Italy

<sup>c</sup>ARPA Friuli Venezia Giulia – OSMER, Visco (Udine), Italy

<sup>d</sup>ARPA Veneto, Servizio Meteorologico, Teolo (Padua), Italy

\*Correspondence to: S. Davolio, Institute of Atmospheric Sciences and Climate (ISAC), National Research Council of Italy (CNR), Via Gobetti 101, Bologna 40129, Italy.

E-mail: S.Davolio@isac.cnr.it

Key words: heavy precipitation, orography, HyMeX, Alps, convection

**ABSTRACT**

During the first HyMeX Special Observation Period (SOP1) field campaign, the target site of North Eastern Italy (NEI) experienced a large amount of precipitation, locally exceeding the climatological values and distributed among several heavy rainfall episodes. In particular, two events that occurred during the last period of the campaign drew our attention. These events had common large-scale patterns and a similar mesoscale setting, characterised by southerly low-level flow interacting with the Alpine orography, but the precipitation distribution was very different. During IOP18 (31 October – 1 November 2012), convective systems were responsible for intense rainfall mainly located over a flat area of the eastern Po Valley, well upstream of the orography. Conversely, during IOP19 (4 – 5 November 2012), heavy precipitation affected only the Alpine area. In addition to IOP18 and IOP19, the present study analyses other heavy-precipitation episodes that display similar characteristics and which occurred over NEI during the autumn of recent years. A high-resolution (2-km grid spacing) non-hydrostatic NWP model and available observations are used for this purpose. The two different observed precipitation patterns are explained in terms of interaction between the impinging flow and the Alps. Depending on the thermodynamic profile, convection can be triggered when the impinging flow is forced to rise over a pre-existing cold-air layer at the base of the orography. In this situation persisting blocked-flow condition and upstream convergence are responsible for heavy rain localized over the plain. Conversely, if convection does not develop, flow-over conditions establish and heavy rain affects the Alps. Numerical parameters proposed in the literature are used to support the analysis. Finally, the role of evaporative cooling beneath the convective systems is evaluated. It turns out that the stationarity of the systems upstream of the Alps is mainly attributable to persisting blocked-flow conditions, while convective outflow slightly modifies the location of precipitation.

1  
2  
3  
4  
5  
6  
7  
8  
9  
10  
11  
12  
13  
14  
15  
16  
17  
18  
19  
20  
21  
22  
23  
24  
25  
26  
27  
28  
29  
30  
31  
32  
33  
34  
35  
36  
37  
38  
39  
40  
41  
42  
43  
44  
45  
46  
47  
48  
49  
50  
51  
52  
53  
54  
55  
56  
57  
58  
59  
60

**1. Introduction**

During autumn 2012, the first field campaign (Special Observation Period - SOP1, Ducrocq et al., 2014) of the international project HyMeX (Hydrological Cycle in the Mediterranean Experiment; Drobinski et al., 2014) took place with the aim of studying heavy precipitation and floods in the Mediterranean basin. The North Eastern Italy hydro-meteorological site (NEI – Figure 1) was selected from the various target areas over the Italian territory monitored during the campaign, in order to specifically investigate Alpine intense rainfall. NEI has the maximum annual-average precipitation over Italy (Frei and Schär, 1998; Isotta et al., 2013) and was also a target site in previous field campaigns (e.g. Mesoscale Alpine Programme, MAP, Bougeault et al. 2001) and projects (e.g. MAP Demonstration Phase - DPHASE, Rotach et al., 2009). Thus, SOP1 represented a sort of continuation of previous experiments, focusing mainly on the finer scales of atmospheric convection.

During autumn, the deepening of Atlantic troughs over the Mediterranean basin and the relatively high sea surface temperature combine to create atmospheric conditions conducive to heavy rainfall (Doswell et al. 1998; Massacand et al., 1998; Buzzi and Foschini, 2000; Borga et al., 2007; Manzato et al., 2015). The steep and complex orography of the Alpine area makes floods a common hazard during autumn. Autumn 2012 was no exception in this regard: several intense precipitation episodes affected NEI, which turned out to be the rainiest area of the campaign (Davolio et al., 2015). More than 1000 mm of rainfall was recorded over the Alps of the Friuli Venezia Giulia (FVG) region (see Figure 1 for the location) during the two-month period of SOP1, locally exceeding climatological values for this time of year. Two contrasting, heavy-precipitation events, thoroughly monitored during Intense Observing Periods (IOPs) 18 and 19, particularly drew our attention and prompted this study.

These two IOPs were very close in time and characterised by similar synoptic conditions and intense low-level south-easterly flow over the Adriatic Sea (typically referred to as Sirocco wind) impinging on the Alps. However, they produced quite different precipitation patterns. In IOP18 (31

1  
2  
3 74 October – 1 November) the development of convective systems was responsible for intense rainfall  
4  
5 75 confined over a flat area of the eastern Po Valley, far upstream of the orography and close to the  
6  
7 76 Adriatic coast. In contrast, during IOP 19 (4 – 5 November) heavy precipitation affected the  
8  
9 77 mountainous Alpine area and only very light rainfall was recorded over the plain.

10  
11 78 Different precipitation patterns associated with similar large-scale circulation were already  
12  
13 79 identified and discussed for the north-western Alps in several studies, fostered by MAP. In  
14  
15 80 particular, the characteristics of two episodes of the MAP field campaign (MAP-IOP2b and MAP-  
16  
17 81 IOP8) were analysed from different perspectives (Rotunno and Ferretti, 2003; Bousquet and Smull,  
18  
19 82 2003; Rotunno and Houze, 2007). It turned out that the different thermodynamic profile of the  
20  
21 83 impinging flow, and thus its different stability, allowed - or prevented - the low-level air from rising  
22  
23 84 over the Alpine barrier. The different orographic flow regime - flow over or flow around (Smith,  
24  
25 85 1979) - determined the location, intensity and characteristics of the precipitation. During MAP-  
26  
27 86 IOP2b heavy orographic rainfall with embedded convection affected the Alpine slopes, while  
28  
29 87 during MAP-IOP8 weak stratiform and long-lasting precipitation was widespread over the Po  
30  
31 88 Valley.

32  
33  
34  
35  
36 89 More recently, Barbi et al. (2012) provided a detailed description of four convective episodes  
37  
38 90 affecting the coastal area of the Veneto region (part of NEI, Figure 1) far from the Alpine  
39  
40 91 orography. These events occurred in September of four consecutive years and the associated large  
41  
42 92 rainfall totals represented a peculiar feature in the climatology of the region, which is characterised  
43  
44 93 by maximum annual values over the Alps and lower annual values, but with high occurrence of  
45  
46 94 heavy rainfall, over the plain. In accordance with the finding of Monai et al. (2006) and Davolio et  
47  
48 95 al. (2009b), the authors highlighted the importance of the orographic flow modification: the south-  
49  
50 96 easterly low-level flow from the Adriatic Sea was blocked and deflected ahead of the Alps,  
51  
52 97 resulting in a north-easterly barrier wind over the plain (Schwerdtfeger, 1984; Di Muzio, 2014).  
53  
54  
55 98 This barrier wind converged with the impinging south-easterly flow near the coastal area and this  
56  
57  
58  
59  
60

1  
2  
3 99 low-level convergence, together with conditionally instability, was responsible for initiating and  
4  
5 100 sustaining organised convection.  
6  
7 101 Conversely, in the NEI Pre-Alpine and Alpine area, higher values of annual accumulated  
8  
9 102 precipitation are closely linked to direct orographic uplift of the southerly moisture-laden airflow  
10  
11 103 from the Adriatic Sea, responsible for long-lasting orographic precipitation. Recent flooding  
12  
13 104 episodes over NEI, also mentioned briefly in Barbi et al. (2012), fit within this category of events,  
14  
15 105 which includes typical autumnal heavy rainfall affecting the southern side of the Alps.  
16  
17 106 In the present study, attention is focussed on the period between September and November, when  
18  
19 107 the climatological peak of heavy precipitation is in the north-western Mediterranean (Ducrocq et al.,  
20  
21 108 2014), and specifically over NEI (Manzato, 2015). This peak is caused by the higher frequency of  
22  
23 109 Atlantic storms entering the Mediterranean and aided by additional heat and moisture provided by  
24  
25 110 the relatively warm Adriatic Sea. Over NEI, during this period there is a progressive transition from  
26  
27 111 summer convective weather, associated with conditionally unstable flow, to the so-called flux  
28  
29 112 precipitation (Manzato, 2007) typical of long-lasting, sometimes flood-producing, events along the  
30  
31 113 southern side of the Alps and associated with near-neutral moist stratification (Miglietta and  
32  
33 114 Rotunno, 2005; Malguzzi et al., 2006).  
34  
35  
36 115 In addition to IOP18 and IOP19 of the HyMeX-SOP1 mentioned above, other heavy-precipitation  
37  
38 116 episodes displaying similar precipitation patterns and affecting NEI are selected and analysed in this  
39  
40 117 study. The aim is to investigate and better understand possible common thermodynamic  
41  
42 118 mechanisms that modulate the precipitation pattern for the two categories of analysed events and to  
43  
44 119 define analytical parameters able to describe the physical processes associated with the two  
45  
46 120 observed orographic flow regimes.  
47  
48  
49 121 The paper is organised as follows. After a description of the employed numerical models and of the  
50  
51 122 simulation strategy (Section 2), the results of a detailed investigation of the events, based on both  
52  
53 123 observations and high-resolution model simulations, are summarised in Section 3. Section 4  
54  
55  
56  
57  
58  
59  
60



124 presents the main findings concerning physical mechanisms playing a key role in different phases  
125 of the events. Finally, conclusions are drawn in Section 5.

## 127 **2. Model description**

128 The Numerical Weather Prediction (NWP) system employed in the present study is based on the  
129 hydrostatic BOlogna Limited Area Model (BOLAM) and the non-hydrostatic MOdello LOcale in  
130 Hybrid coordinates (MOLOCH), developed by the Institute of Atmospheric Sciences and Climate  
131 of the Italian National Research Council (CNR – ISAC). The two models are being used  
132 operationally at ISAC as part of an agreement with the National Civil Protection Department and  
133 also at various Italian national agencies and regional meteorological services. BOLAM and  
134 MOLOCH differ in their dynamical core, including a different choice for their vertical coordinate  
135 sets, and by the fact that BOLAM includes a parameterization for deep convection, based on a  
136 modified version of the Kain-Fritsch scheme (Kain, 2004). In MOLOCH deep convection is  
137 explicitly simulated and a simple shallow convection scheme is applied. BOLAM (horizontal  
138 resolution 11 km, 50 vertical levels) is run over a European domain and it is mainly employed to  
139 provide lateral boundary conditions for the inner grid (horizontal resolution 2.3 km and 54 vertical  
140 levels) of MOLOCH (Figure 1) at 1-hour intervals. This intermediate nesting step has proved to be  
141 reliable and economical in bridging the gap between the coarse-resolution global model fields  
142 (0.25°/6-hourly ECMWF analysis data) and the high-resolution forecasts (Buzzi et al., 2014).  
143 Therefore only a brief description of the MOLOCH model is provided here. For a description of  
144 BOLAM refer to Buzzi et al. (2003), Malguzzi et al. (2006) and Davolio et al. (2013).  
145 MOLOCH is a non-hydrostatic, fully compressible, convection-permitting model (Malguzzi et al.,  
146 2006; Buzzi et al., 2014). It integrates the set of atmospheric equations with 12 prognostic variables  
147 — pressure, absolute temperature, specific humidity, horizontal and vertical components of  
148 velocity, turbulent kinetic energy and five water species (cloud water, cloud ice, rain, graupel and  
149 snow) — represented on the latitude–longitude, rotated Arakawa C-grid. It employs a hybrid

1  
2  
3 150 terrain-following vertical coordinate, depending on air density and smoothing to horizontal surfaces  
4  
5 151 at higher altitudes. Time integration is based on an implicit scheme for the vertical propagation of  
6  
7 152 sound waves, while explicit time-splitting schemes are implemented for integration of the  
8  
9 153 remaining terms of the equations of motion. Three-dimensional advection is computed using the  
10  
11 154 Eulerian weighted average flux scheme (Billet and Toro, 1997). The physical parameterisation  
12  
13 155 schemes are common between the two models. The microphysical scheme is based on the  
14  
15 156 parameterisation proposed by Drofa and Malguzzi (2004). Atmospheric radiation is computed with  
16  
17 157 a combined application of the Ritter and Geleyn (1992) scheme and the ECMWF scheme  
18  
19 158 (Morcrette et al., 2008). The turbulence scheme is based on a turbulent kinetic energy – mixing  
20  
21 159 length ( $E-l$ ) order 1.5 closure theory (Zampieri et al., 2005). The soil model uses seven layers and it  
22  
23 160 takes into account the observed geographical distribution of different soil types and soil physical  
24  
25 161 parameters. For a more detailed description of MOLOCH refer to Buzzi et al. (2014).  
26  
27  
28  
29 162 In the present study, the NWP system was applied to six case studies (Table 1). First, a thorough  
30  
31 163 verification of the simulations was performed in order to verify that the model correctly reproduced  
32  
33 164 the main dynamical features of each event. Model simulations were compared with observations,  
34  
35 165 such as the dense ground-based station networks (which observed near-surface temperature, wind,  
36  
37 166 humidity and precipitation), radiosoundings and operational wind profilers over northern Italy, in  
38  
39 167 order to assess the mesoscale features. The large-scale dynamics was compared against ECMWF  
40  
41 168 analyses. No special observations, except for some additional soundings, were available over the  
42  
43 169 NEI area for IOP18 and IOP19 events. However, it is worth mentioning that the unprecedented  
44  
45 170 collaboration fostered by the HyMeX-SOP1 among research institutions and regional  
46  
47 171 meteorological centres and agencies (Davolio et al., 2015) allowed a fruitful collaboration and  
48  
49 172 sharing of observation database (national radar composite and raingauge network, among others).  
50  
51  
52 173 For the sake of brevity, only the comparisons concerning the total precipitation are presented.  
53  
54  
55 174 For each case study, different initialization times for BOLAM and for MOLOCH nesting were  
56  
57 175 tested and the best simulation was chosen as the “control run” to investigate each episode. We made  
58  
59  
60

1  
2  
3 176 this choice to ensure that the simulation is as close to reality as possible, in terms of location,  
4  
5 177 intensity and evolution of the precipitation, as well as of triggering and organization of the  
6  
7 178 precipitating systems, so as to investigate the physical mechanisms rather than the skill of  
8  
9 179 operational forecasting.  
10  
11  
12 180

### 13 181 **3. Heavy precipitation events over NEI**

14  
15  
16 182 A brief description of the selected events, listed in Table 1, is provided here, based on model  
17  
18 183 simulations and comparisons against available observations. The model simulations are used to  
19  
20 184 investigate the physical mechanisms responsible for the precipitation events in Section 4.

21  
22  
23 185 From a preliminary analysis, it turned out that all the selected events were driven by similar large-  
24  
25 186 scale conditions (Figure 2), i.e. a synoptic scale trough extended over the Mediterranean and the  
26  
27 187 low-level flow was southerly, coming from the Adriatic Sea. Moreover, during the initial stage of  
28  
29 188 the events the mesoscale flow features were also similar. The pre-existing cold air over the plain of  
30  
31 189 NEI enhanced the low-level blocking caused by the incoming flow damming up against the Alps  
32  
33 190 (Di Muzio, 2014). This produced a strong deflection (flow around) of the southerly flow by the  
34  
35 191 Alps, causing a barrier wind (Buzzi, 2004). This deflection produced north-easterly wind at the foot  
36  
37 192 of the Alps, initially preventing the warm air from advancing inland towards the mountains.

38  
39  
40 193 The analysis of the events also showed that, after the initial stage, different mesoscale evolutions  
41  
42 194 were responsible for the different precipitation patterns already mentioned (the low-level flow  
43  
44 195 evolution is thoroughly analysed in Section 4.2). This led us to separate the events into two main  
45  
46 196 categories. Hereafter we refer to “Alpine” events that were characterised by heavy, widespread  
47  
48 197 rainfall over the Alpine area, associated with uplift of the southerly low-level flow over the  
49  
50 198 orographic barrier, which represents the most frequent case in such situations. In addition to IOP19,  
51  
52 199 two recent heavy-precipitation episodes affecting the Alps were also analysed (Table 1). In contrast,  
53  
54 200 we refer to “Upstream” events that were characterised by intense and almost stationary convective  
55  
56 201 precipitation over the plain upstream of the orography, associated with persisting low-level  
57  
58  
59  
60

1  
2  
3 202 blocking of the impinging southerly flow. In addition to IOP18, two Upstream events were selected  
4  
5 203 among those discussed in Barbi et al. (2012). However, since the interest is placed on  
6  
7 204 orographically modified flow, we have not considered the other two cases included in the study of  
8  
9 205 Barbi et al. (2012), which were similar in terms of precipitation distribution but characterised by  
10  
11 206 north-easterly Bora wind instead of barrier-type wind.  
12  
13  
14 207 Generally, simulated rainfall showed a better agreement with the observations for the Alpine  
15  
16 208 (Figures 3 and 4 (a), (b), (c)) rather than the Upstream events (Figures 3 and 4 (d), (e), (f)). The  
17  
18 209 direct orographic uplift, which represents a fairly large-scale forcing, is probably better simulated  
19  
20 210 by the model than the local triggering of convection, and may thus account for the larger degree of  
21  
22 211 predictability.  
23  
24  
25 212  
26  
27 213 **3.1 IOP19**  
28  
29 214 By 4 November 2012, an upper-level trough extended from the Scandinavian Peninsula to the  
30  
31 215 Atlantic Ocean, with a surface pressure minimum close to Ireland. The Mediterranean was affected  
32  
33 216 by intense south-westerly flow in the middle troposphere, while a warm conveyor belt ahead of the  
34  
35 217 cold front advected warm air towards the Italian peninsula (Ferretti et al., 2014). At the surface, the  
36  
37 218 development of a shallow cyclone over the Gulf of Lion, progressively moving towards northern  
38  
39 219 Italy, favoured intense low-level warm and moist southerly flow over the Adriatic Sea. The  
40  
41 220 synoptic pattern (Figure 2(a)) evolved slowly during 4 and 5 November, due to the presence of a  
42  
43 221 pressure ridge over eastern Europe, and was associated with intense precipitation over NEI (Figure  
44  
45 222 3(a)), especially in the areas close to the Slovenian border, where a maximum of 370 mm in about  
46  
47 223 24 hours was observed. While the precipitation was very weak over the plain, intense rainfall,  
48  
49 224 exceeding 200 mm in 24 hours, was recorded over a wide area of the Alps. However, only a few  
50  
51 225 lightning strikes were detected indicating that the precipitation was mainly stratiform/orographic in  
52  
53 226 nature. This is also supported by low Convective Available Potential Energy (CAPE) values, and  
54  
55 227 moderate vertical motion was only attained during the final phase of the event, as indicated by both  
56  
57  
58  
59  
60

model simulations and data from the Campoformido (Udine) radiosounding (location in Figure 1). MOLOCH correctly simulates the rainfall distribution (Figure 4(a)), although it slightly underestimates the orographic rainfall. Also, the hourly rainfall evolution is in good agreement with radar estimates (not shown), with the heaviest precipitation occurring in the evening over the northeasternmost sector of NEI Alps. The model simulates a slightly faster passage of the cold front over the area, thus sweeping away the precipitation system about two hours earlier than observed. On the mesoscale, it is worth mentioning that in the initial phase of the event, cold air was present over the plain (average  $\theta_e$  was 313 K close to the ground), and a barrier wind developed ahead of the Alps, due to the westward deflection of the southerly wind coming from the sea, as predicted by MOLOCH and confirmed by wind measurements taken just inland of the Adriatic coast (not shown). The inflow from the sea was initially forced to rise over the cold air. Later, while increasing its intensity, the southerly flow was characterised by a gradual transition from flow-around to flow-over conditions, associated with the removal of the cold air at the base of the orography. The uplift was then directly forced by the passage over the Alps, where most of the precipitation occurred (Figure 3(a)).

243

### 244 3.2 Piancavallo 2012

Between 10 and 11 November 2012, just a few days after the end of the SOP1, a trough deepened over the Iberian Peninsula (Figure 2(b)), reaching Northern Africa and activating intense warm and moist south-westerly flow over the central Mediterranean. The eastward evolution of the trough was very slow and a cut-off low eventually formed over Spain. The low-level moist flow over the Adriatic Sea produced heavy rainfall (almost 400 mm in 24 hours) over the Pre-Alpine area (Figure 3(b)), between Veneto and FVG regions, while precipitation was light over the plain. MOLOCH correctly simulates the orographic precipitation (Figure 4(b)) although the maximum accumulation is underestimated by about 20% (310 mm instead of 390 in 24 hours at Piancavallo, over the FVG Alps; Table 1). Similar to IOP19 event, the Sirocco wind, initially deflected ahead of the Alpine

1  
2  
3  
4  
5  
6  
7  
8  
9  
10  
11  
12  
13  
14  
15  
16  
17  
18  
19  
20  
21  
22  
23  
24  
25  
26  
27  
28  
29  
30  
31  
32  
33  
34  
35  
36  
37  
38  
39  
40  
41  
42  
43  
44  
45  
46  
47  
48  
49  
50  
51  
52  
53  
54  
55  
56  
57  
58  
59  
60

barrier, progressively penetrated inland, gently rising over the Alps. Again, this wind pattern is confirmed by SODAR wind profile measurements (not shown). During the most intense phase of the event, MOLOCH simulates vertical velocities of a few  $\text{m s}^{-1}$  within the precipitation system, indicating the probable development of embedded convection.

**3.3 Vicenza 2010**

This event was a long-lasting episode of intense precipitation, leading to a major river flood in the city of Vicenza (location in Figure 1). After weak rainfall during the morning of 31 October 2010, moderate to heavy precipitation developed over the Pre-Alpine area, persisting into 1 November, while only weak rainfall affected the plain. As in the previous cases, rainfall was associated with a deep trough over the Mediterranean basin (Figure 2(c)), evolving into a cut-off low over the Gulf of Lion in the final phase. A reinforcing ridge over eastern Europe slowed the eastward progression of the trough, thus favouring the stationarity of the intense low-level Sirocco wind over the Adriatic Sea and the persistence of precipitation. The location of intense rainfall was strictly correlated with orographic features along a WSW-ENE direction over the Pre-Alps (Figure 3(c)) and the pattern did not change throughout 31 October and 1 November. The most intense phase of the event was characterised by rainfall reaching 460 mm in 48 hours in Veneto and about 600 mm in 48 hours in FVG. However, considering the whole 72-hour period of rainfall, more than 700 mm were recorded in FVG and more than 500 mm in several stations in the Veneto region. As shown in Figure 4(c) MOLOCH correctly simulates the precipitation pattern, displaying intense rainfall over the Alps. The hourly evolution (not shown) is properly simulated, with increasing rain rate in the morning of 1 November, possibly associated with embedded convective activity, and rainfall progressively weakening in the afternoon, eventually becoming scattered. Also in this case, the initially weak low-level south-easterly flow from the Adriatic Sea was blocked and deflected as a barrier wind, but as it increased in intensity, it was able to flow over the Alps. This feature is confirmed by

279 SODAR wind profile observations (Figure 5(a)) taken in Concordia Sagittaria close the Adriatic  
280 coast (location in Figure 1).

281

### 282 3.4 IOP18

283 On the morning of 31 October 2012, a secondary cyclone developed over Spain, embedded in a  
284 larger cyclonic circulation centred north of the British Isles. This low-pressure system moved  
285 eastward over the Gulf of Lion reaching Corsica in the afternoon (Figure 2(d)) and inducing low-  
286 level south-easterly moist unstable flow over the Adriatic area, impinging on the Alps, and south-  
287 westerly flow aloft. In contrast to the previous events, here the low-level intense currents over the  
288 Adriatic basin were not able to pass over the Alps during the whole event and the persisting  
289 convergence line between the Sirocco wind and the barrier wind focused the convective activity  
290 over the Veneto plain, just north of the Po river outlet. Radar images (not shown) revealed that  
291 initially the rainfall was produced in the early afternoon of 31 October by convective systems  
292 triggered over the Adriatic Sea and then advected inland over the Po Valley. This phase of the event  
293 is reproduced with some delay in MOLOCH, which simulates intense rainfall over the plain only  
294 after 1700 UTC. Later in the evening of 31 October, almost stationary convection developed over  
295 the plain, related to the convergence line. Although the complete picture of simulated rainfall is  
296 affected by a significant error in the location (Figure 4(d)), the simulation captures correctly the  
297 dynamical evolution of the low-level flow and of the convergence line, as well as the total rainfall.  
298 Therefore, the model reproduces the convective activity and its stationarity, but slightly later than  
299 observed. In less than 12 hours, intense precipitation exceeding 120 mm affected a restricted area of  
300 NEI (Figure 3(d)). For some raingauge stations the return period of the event was calculated to be  
301 longer than 50 years. However, the rapid eastward progression of the cyclone moved the  
302 precipitation away. Observation revealed that wind gusts over the Adriatic exceeded  $80 \text{ km h}^{-1}$  (not  
303 shown) and a major storm surge affected the NEI coast.

304



1  
2  
3  
4  
5  
6  
7  
8  
9  
10  
11  
12  
13  
14  
15  
16  
17  
18  
19  
20  
21  
22  
23  
24  
25  
26  
27  
28  
29  
30  
31  
32  
33  
34  
35  
36  
37  
38  
39  
40  
41  
42  
43  
44  
45  
46  
47  
48  
49  
50  
51  
52  
53  
54  
55  
56  
57  
58  
59  
60

**3.5 Marghera 2007**

This event, thoroughly described and investigated in Davolio et al. (2009b) and Rossa et al. (2010), was the most intense rainfall episode that occurred during the operational period of the MAP-DPHASE project (Rotach et al., 2009). It was responsible for a severe, although localised, flood over a flat area near Venice (location in Figure 1) on 26 September 2007. It was associated with a stationary mesoscale convective system (MCS) that developed west of the Venice lagoon (Barbi et al., 2012), and took a V-shape in infrared satellite imagery (Setvák et al., 2013). More than 320 mm fell in less than 12 hours (Figure 3(e)), of which more than 240 mm fell in only 3 hours. An upper-level trough, deepening over France and the Mediterranean while approaching the western Alps (Figure 2(e)), favoured orographic cyclogenesis over the Gulf of Genoa and produced a south-westerly diffluent flow over NEI. The orographically-induced cyclone enhanced the south-easterly low-level jet over the Adriatic Sea, which was deflected in front of the Alpine barrier. The MCS was triggered along the convergence line between the Sirocco wind and the barrier wind. MOLOCH simulates scattered convective activity in the early morning, turning into organised convection able to produce large rain rate up to  $180 \text{ mm h}^{-1}$  close to the Venice lagoon (Figure 4(e)). Low-level convergence, stationary convection, as well as the orientation of the V-shape structure of the MCS are correctly simulated. Differences between the structure of the observed and forecast rainfall fields remain within the expected variability for this particular event, as discussed in Davolio et al. (2009). Finally, the persistence of blocked-flow conditions and of the barrier wind over the NEI plain is confirmed by SODAR observations (Figure 5(b)) taken close to the city of Padua (location in Figure 1).

**3.6 Mira 2009**

On 16 September 2009 the synoptic circulation was characterised by a cyclonic disturbance over the western Mediterranean basin (Figure 2(f)) and south-westerly flow in the middle troposphere over NEI. The cut-off cyclone centred between Spain and France induced moist south-easterly flow



in the lower levels over the Adriatic Sea. Again, the interaction between the north-easterly barrier wind in front of the Alps and the Sirocco wind produced a convergence pattern able to trigger convective activity over the Veneto plain, close to the Venice lagoon. In the early morning convective cells moved from the Adriatic Sea towards the Pre-Alpine ridge and later became more stationary, regenerating along the coastal area. Around 1200 UTC, a stationary MCS developed producing intense rainfall. This evolution explains the precipitation pattern shown in Figure 3(f) characterised by a main maximum of about 180 mm in 24 hours close to the coast and weaker localised maxima over the Pre-Alps. The MOLOCH simulation of this event is not completely satisfactory (Figure 4(f)), but reproduces the most intense phase of stationary convection around 1200 UTC, which is the most relevant aspect for this study. Indeed, a rainfall maximum is simulated over the plain, although displaced south-westward and less intense of the maximum over the orography.

#### 4. Physical mechanisms

##### 4.1 Theoretical framework

The cases summarised in Section 3 are characterised by the interaction of moist and warm flow with a mountain ridge. Before presenting a detailed investigation of the events in terms of physical mechanisms and numerical parameters, a brief review of the main scientific achievements in the field of orographically modified flow and orographic precipitation is provided, highlighting the framework and motivation of the present study.

Idealised studies of stably-stratified dry flows impinging on a mountain ridge revealed the Froude number ( $Fr = U/(N \cdot h)$  where  $U$  is a measure of the wind speed,  $h$  is a typical height of the mountain and  $N$  is the static stability) as the main parameter able to discriminate between a “flow-over” regime, when the flow passes over the ridge without being significantly deflected ( $Fr > 1$ ), and a “flow-around” regime, when the flow is blocked in the lower layers and deflected by the ridge ( $Fr < 1$ ) (Smolarkiewicz and Rotunno, 1990). Pierrehumbert and Wyman (1985) evaluated the upstream

1  
2  
3 357 influence of the orography and showed that upstream blocking and flow diversion in a rotating  
4  
5 358 atmosphere is strictly connected with barrier winds that are generated as a consequence of the  
6  
7 359 damming of low-level stable air. This aspect is particularly relevant as a theoretical support for the  
8  
9 360 observed phenomenon of barrier wind over NEI described in Section 3.  
10  
11 361 The introduction of moisture, which modifies the “effective” static stability  $N$  of the air at  
12  
13 362 saturation and hence the dynamical response to orographic forcing, depending on when and where  
14  
15 363 condensation occurs, may favour the flow-over regime (e. g. Miglietta and Buzzi, 2004). In the last  
16  
17 364 decade, attention has been mainly focussed on conditionally unstable moist flow and on regimes of  
18  
19 365 convection propagation in presence of orography, pointing out the limited applicability of  $Fr$  in such  
20  
21 366 conditions. Chen and Lin (2005) and Miglietta and Rotunno (2009) found that  $Fr$  taken alone is  
22  
23 367 unsuitable to explain the precipitation distribution in a convective environment. Thus, Miglietta and  
24  
25 368 Rotunno (2009, 2010) introduced several non-dimensional parameters to account for orographic  
26  
27 369 triggering of convection in conditionally unstable flow and subsequent interactions between the  
28  
29 370 environmental flow and the convective cold pool. In particular, the parameter  $h_m/LFC$ , namely the  
30  
31 371 ratio between ridge height ( $h_m$ ) and the altitude of the level of free convection (LFC), was suggested  
32  
33 372 to quantify the likelihood that orographic lifting is sufficient to initiate convection.  
34  
35 373 In addition to idealised simulations, important results came also from case studies analyses, mostly  
36  
37 374 fostered by field campaigns (Rotunno and Houze, 2007). Buzzi and Foschini (2000) and Rotunno  
38  
39 375 and Ferretti (2001, 2003) identified important aspects of Alpine heavy rainfall episodes, both at the  
40  
41 376 synoptic- and meso-scale, like the presence of low-level jets and along-ridge gradients of relative  
42  
43 377 humidity able to influence flow ascent through condensation and latent heating. More recently, the  
44  
45 378 dynamics of a low-level moist jet interacting with a complex-shaped ridge has been studied in  
46  
47 379 Nuissier et al. (2008) and Bresson et al. (2009, 2012). They showed that the location of convection  
48  
49 380 triggering and the characteristics of the MCS, in terms of stationarity and accumulated rainfall,  
50  
51 381 depend on different environmental parameters, such as ridge shape, low-level horizontal wind and  
52  
53 382 humidity profiles, CAPE and upstream cold pool features. Finally, the characterisation of the  
54  
55  
56  
57  
58  
59  
60

environment associated with heavy precipitation, in particular concerning the thermodynamic properties of the low-level jet, has been also explored through a climatological approach (Rudari et al., 2004; Ricard et al., 2012).

In analogy with the above-mentioned findings, we tried to apply the theoretical results to the observed cases, in order to identify parameters able to describe the different behaviour observed for Upstream and Alpine events. However, it is worth bearing in mind that in real case studies the environment is more complex than in idealized experiments.

## 4.2 Overview of the dynamical evolution

The dynamical characteristics of the flow interacting with the Alpine orography are preliminarily investigated computing the moist Fr using a vertical profile obtained as an average over an area of about 50 x 50 km centred in 45 °N – 13 °E (shown in Figure 7). This area, located in the middle of the northern Adriatic Sea, is chosen to sample the mesoscale incoming flow upstream of the orography. Fr is computed every three hours, starting from the onset of impinging flow and until the flow in the area can be considered not yet perturbed by the interaction with the orography or by the occurrence of intense rainfall. However, several drawbacks emerge preventing us from the possibility to identify clearly the two separate classes of events using Fr. In fact, in addition to the known difficulties arising in Fr computation in the case of conditionally unstable flow (Miglietta and Rotunno, 2009), even for almost stratified flow as in the Alpine events results do not completely meet expectations. Fr is computed using  $h = 2000$  m for orography height, averaging the meridional component of the wind over the model levels up to this height, and evaluating the flow stability as suggested in Barrett et al. (2014):

$$N^2 = \frac{g}{\theta_t} \frac{\theta_t - \theta_b}{h}$$

where  $g = 9.81 \text{ m s}^{-2}$  while  $\theta_b$  and  $\theta_t$  are respectively virtual potential temperature at the lowest model level and at the model level corresponding to about 2000 m. Fr values barely exceed one

1  
2  
3 408 (Figure 6), as it would be expected in case of flow-over regime. However, a more detailed analysis  
4  
5 409 reveals a strong horizontal gradient of  $Fr$  values across the Adriatic basin for the Alpine events, and  
6  
7 410 thus a strong sensitivity to the selected area of computation. In particular,  $Fr$  values much larger  
8  
9 411 than unity are found on the eastern side of the Adriatic basin, while values lower than unity  
10  
11 412 characterise the flow close to the Italian coast. Thus, instead of considering the absolute  $Fr$  value,  
12  
13 413 whose computation may be somewhat arbitrary, the attention is focused on its evolution in time.  
14  
15 414 Figure 6 shows that for all the three Alpine events  $Fr$  steadily and substantially increases during the  
16  
17 415 event. This is consistent with blocked-flow and barrier wind conditions at the beginning of the  
18  
19 416 event and a gradual change towards a flow-over regime, starting from the easternmost part of the  
20  
21 417 Alps, as simulated by MOLOCH and confirmed by available observations (soundings and wind  
22  
23 418 profilers, e.g. in Figure 5(a)). On the other hand, for the Upstream events and especially for M2007  
24  
25 419 and M2009 cases,  $Fr$  values remain low, hardly exceeding 0.6. The exceptionally strong wind  
26  
27 420 attained during IOP18 is responsible for a temporary increase of  $Fr$ , although not higher than 0.8.  
28  
29 421 However, in this latter case, the low-level wind is also steered by the mesoscale cyclonic circulation  
30  
31 422 that forces its rotation from the Adriatic Sea into the Po Valley, thus favouring the blocking effect  
32  
33 423 of the Alps. It is also worth noting that  $Fr$  for the Alpine events is generally larger than the value  
34  
35 424 obtained for the Upstream events, thus suggesting a different flow regime. Therefore, although the  
36  
37 425 absolute value of  $Fr$  does not provide critical information, relative values between different events  
38  
39 426 seem to be able to describe different dynamical characteristics of the analysed events.  
40  
41 427 Keeping in mind these results and the theoretical background briefly described in Section 4.1, the  
42  
43 428 analysis is focussed on two different phases of the events: (i) the triggering phase, being the initial  
44  
45 429 period characterised by the possible development of convective cells and precipitation initiation; (ii)  
46  
47 430 the precipitation phase, when the precipitating system is well developed. For the sake of brevity and  
48  
49 431 clarity, most of the results are presented only for two events, representative of the two categories:  
50  
51 432 V2010 for Alpine events and M2007 for Upstream events.  
52  
53 433  
54  
55  
56  
57  
58  
59  
60

### 4.3 The triggering phase

During the initial phase of both events, the low-level wind field (Figures 7 (a), (b)) displays a similar pattern, characterised by blocked flow upstream of the Alps, possibly enhanced by the presence of pre-existing cold air (Pierrehumbert and Wyman, 1985), producing a north-easterly barrier wind over the NEI plain and over the Po Valley. The convergence between the barrier wind and the Sirocco wind from the Adriatic Sea clearly show up in Figure 7 as a narrow zone of low wind speed. However, the consequence of this convergence is quite different, as shown by the cross sections drawn along the direction of the impinging flow. On one hand, for V2010 case (Figure 8(a)) the moist south-easterly flow gently rises over the cold layer located at the foot of the Alps where the barrier wind is blowing, before being further lifted over the orography. No precipitation is associated with the uplift during this phase. On the other hand, in M2007 event (Figure 8(b)) convection is triggered in correspondence with the ascent over the barrier wind cold layer and intense precipitation is suddenly produced.

This different behaviour has a critical impact on the following dynamical evolution, when the intensity of the impinging flow increases in response to the approaching synoptic disturbance. As shown in Figures 7(c), in V2010 southerly flow progressively penetrates into the plain, the cold barrier wind layer disappears and the flow eventually passes over the Alps. All over the eastern Alps the 10-m wind field displays a clear flow-over pattern in response to increasing wind speed, while the flow stability remains nearly constant. Consequently, precipitation affects mountainous areas where uplift and condensation occur. The cross section (Figure 8(c)) also indicates some small-scale and intense vertical motions over the orography, possibly due to embedded convective activity that locally enhances rainfall intensity.

Conversely, the convergence pattern along the coastal area persists in M2007 (Figure 7(d)). The blocking conditions persist, consistent with the result of the Fr analyses, the low-level flow does not penetrate inland and deep convection intensifies (Figure 8(d)), fed by moist and warm air from the Adriatic Sea. This resembles the blocked-flow condition considered as the most favourable to heavy

1  
2  
3 460 rainfall rates in the idealised experiments shown in Miglietta and Rotunno (2014) and in Davolio et  
4  
5 461 al. (2009a), characterised by a convective cold pool propagation nearly countered by the  
6  
7 462 environmental wind. The role of the evaporative cold pool is further discussed in Section 4.5.  
8  
9 463 Now that the general physical mechanisms have been described, a more detailed thermodynamic  
10  
11 464 analysis concerning the initial triggering phase of the events is performed. First, vertical  
12  
13 465 thermodynamic profiles are analysed (Figures 9(a), (b)). Profiles are not computed for a single grid  
14  
15 466 point but as an average over an area of about 15 x 15 km over the northern Adriatic Sea, almost  
16  
17 467 contained in the area used for computing Fr. Using an upstream area gives a better sampling of  
18  
19 468 undisturbed flow characteristics before its interaction with the orography and with the cold pool  
20  
21 469 producing uplift and possibly triggering convection. Profiles are computed for the initial phase of  
22  
23 470 the events, when convection is possibly being triggered but intense precipitation has not started yet.  
24  
25 471 These profiles allow for the evaluation of the LFC height and CAPE (using the most unstable  
26  
27 472 parcel) and several indices related to stability (Tables 2 and 3). Similarly, vertical profiles over the  
28  
29 473 NEI plain, together with the analysis of cross sections similar to those presented in Figure 8,  
30  
31 474 provide the estimate of  $h_b$  as the top of the layer characterised by stable stratification and north-  
32  
33 475 easterly wind. This layer is found to be quite shallow, with its depth always being lower than 800  
34  
35 476 m.  
36  
37 477 Although it is possible to identify an LFC located at a relatively high elevation, around 1000  
38  
39 478 meters, the profile for V2010 (Figure 9(a)) shows a nearly neutral moist vertical stratification of the  
40  
41 479 air mass, even stable in the lower layers and with very low CAPE values (below  $50 \text{ J kg}^{-1}$ ). This is a  
42  
43 480 common characteristic among the Alpine events, with the LFC being even higher in IOP19. The  
44  
45 481 wind veers by about 45 degrees over the lowest 2 km. The moisture content is already high at the  
46  
47 482 beginning of the simulation and the air column becomes saturated quite quickly during the first day  
48  
49 483 of the event (not shown), without relevant changes in stability properties. On the other hand, for  
50  
51 484 M2007 (Figure 9(b)) and similarly for M2009 (not shown) the atmosphere is conditionally unstable,  
52  
53 485 close to saturation in the lowest layers and much drier above 850 hPa where the wind direction  
54  
55  
56  
57  
58  
59  
60

1  
2  
3 486 abruptly changes from south-easterly to south-westerly. The LFC is fairly low, being located below  
4  
5 487 500 m and the value of CAPE is relevant, greater than  $1000 \text{ J kg}^{-1}$ . It is worth mentioning that the  
6  
7 488 vertical profile for IOP18 (not shown) is also characterised by a low LFC. However, moisture is  
8  
9 489 higher and more uniform all over the troposphere and CAPE is lower and mainly concentrated in  
10  
11 490 the lower layers, as usually observed for autumn events with respect to late summer cases.  
12  
13  
14 491 The described behaviour is also in agreement with positive values of the Lifted Index (Galway,  
15  
16 492 1956) ( $\text{LI} > 2.2 \text{ K}$ , in Table 2) found for the Alpine events, which indicate stable conditions during  
17  
18 493 the initial phase of the event. For the Upstream events (Table 3) potential instability is instead  
19  
20 494 present. This is especially true for M2007 and M2009 events, which have a negative LI, but also for  
21  
22 495 IOP18, even if the LI indicates nearly neutral conditions ( $0.5 \text{ K}$ ). Indeed, referring to a  
23  
24 496 climatological statistical analysis of convective events over the FVG area (Manzato, 2003) a LI of  
25  
26 497  $+0.64 \text{ K}$  represents the discriminant value to classify convection development in the FVG plain.  
27  
28  
29 498 While it is evident that deep convection cannot develop in the initial stage of the Alpine events, the  
30  
31 499 Upstream events deserve a further analysis of the triggering phase. Among the relevant parameters  
32  
33 500 modulating rainfall rate and location for a conditionally unstable flow over a ridge, Miglietta and  
34  
35 501 Rotunno (2009) suggested to use the ratio of mountain height to the level of free convection  
36  
37 502 ( $h_m/\text{LFC}$ ). This parameter evaluates whether the uplift forced by the mountain is sufficient to allow  
38  
39 503 air parcels to reach their LFC and thus to trigger convection. In the present analysis the same idea is  
40  
41 504 adopted, but considering the cold layer with barrier wind, instead of the mountain, as the “obstacle”  
42  
43 505 providing the initial uplift forcing. A similar approach was used by Mazòn and Pino (2013) in their  
44  
45 506 analysis of convective cloud bands developing near the Mediterranean coasts. In other words, this  
46  
47 507 cold layer located upstream of the orography, and characterised by the barrier wind, acts as an  
48  
49 508 “effective mountain” (Lin et al., 2005) of height  $h_b$ .  
50  
51  
52 509 Values of  $h_b/\text{LFC}$  computed for the three Upstream events during the triggering phase are close to  
53  
54 510 or greater than unity, consistent with the fact that convection is triggered where the impinging and  
55  
56 511 barrier flows meet. For IOP18, besides the main rainfall episode that occurs in the late evening  
57  
58  
59  
60



1  
2  
3  
4  
5  
6  
7  
8  
9  
10  
11  
12  
13  
14  
15  
16  
17  
18  
19  
20  
21  
22  
23  
24  
25  
26  
27  
28  
29  
30  
31  
32  
33  
34  
35  
36  
37  
38  
39  
40  
41  
42  
43  
44  
45  
46  
47  
48  
49  
50  
51  
52  
53  
54  
55  
56  
57  
58  
59  
60

(associated with the highest value of  $h_b/LFC$ ), an interesting convective phase in the morning is also considered, when shallow convective activity developed over the Adriatic Sea in correspondence with the aforementioned convergence line. Also in this case  $h_b/LFC$  is close to unity. However, during IOP18, convection is triggered but does not develop into deep convection. Instead, for M2007 and M2009 events, high values of CAPE indicate favourable conditions for vigorous convective vertical motions and heavy rainfall.

Another clear indication concerning the type of event can be obtained by considering the buoyancy of air parcels displaced vertically from multiple levels (Davolio et al., 2009a; Buzzi et al., 2014). At each model level, the virtual temperature of an air parcel adiabatically raised by a given displacement is computed and compared with the virtual temperature of the environment at the new altitude. Since early stages of convection are analysed, computation assumes the loading of condensed water (reversible uplift), considers the occurrence of precipitation negligible, and entropy conservation of a mixture of air/vapour/cloud water. The virtual temperature difference between the parcel and the environment, is used to calculate the buoyancy as follows:

$$B = g \frac{T_v^{par} - T_v^{env}}{T_v^{env}}$$

Buoyancy is computed as a function of the height of the parcel, thus providing a buoyancy profile relative to more parcels. Figure 10 shows the results for a vertical lift of 500 metres. Similar results hold for slightly different vertical displacements (consistent with the height of the leading edge of the barrier-wind cold layer), small enough to assume that condensed water is still retained by the lifted parcel. The Upstream convective cases are characterised by positive buoyancy, and thus instability to small vertical displacements in the lowest atmospheric layer of depth of roughly 1000 metres. The vertical profile of buoyancy for IOP18 is characterised by larger values close to the ground, progressively decreasing aloft. This is consistent with thermodynamic profiles close to saturation, unstable in the lower layers and almost neutral above, with moderate CAPE values. Conversely, M2007 and M2009 thermodynamic profiles (Figure 9(b)) indicate increasing relative



humidity with height in the first 1500 metres, characterised by a lapse rate close to the dry adiabatic. Thus buoyancy shows that the most unstable parcels are located at around 500 metres above the surface and not near the ground. Conversely, buoyancy presents negative values for the Alpine events, indicating overall stable conditions. The buoyancy profile for IOP19 is slightly different between 1000 and 2000 m, but still representative of stability to vertical displacements. In summary, the thermodynamic profile of the impinging southerly flow, which is forced to rise over the cold stable layer located over the plain upstream of the orography, determines the different behaviour observed in the two classes of event.  $h_b/LFC$  reveals the possible triggering of convection during the first phase of the events, in case of conditional instability. Also LI turns out to be important because it indicates a necessary condition for potential instability in order to realise vigorous convective activity. Once convection is initiated, its intensity is related to CAPE.

#### 4.4 Precipitation phase: Alpine events

As previously described, if convection is not triggered in correspondence with convergence and uplift, the south-easterly flow is able to progressively penetrate towards the Alps, replacing the pre-existing cold air ahead of the orography. Consistently, a gradual transition from blocked-flow to flow-over conditions is observed. However, model simulations (see for example the cross section in Figure 8(c)), as well as rainfall and remote sensing observations, reveal that convective activity can be embedded in the orographic precipitation, at least in the most intense phase of the events. This is a quite typical characteristic of heavy-precipitation events over north-eastern Alps, usually referred to as flux precipitation (Manzato, 2007), that deserves further investigation.

As presented in Section 4.2 for the Alpine episodes, variation of Fr describes the transition to a more pronounced flow-over conditions during the event. Moreover, an analysis of the thermodynamic vertical profiles upstream of the orography reveals that the impinging flow becomes progressively more unstable, and during the precipitation phase slightly unstable conditions are attained. Therefore, the parameter  $h_m/LFC$  becomes suitable to explain the possible

1  
2  
3 563 occurrence of convective activity. In Figure 11, the evolution in time of  $h_m/LFC$  is plotted for the  
4  
5 564 Alpine events. Values of  $h_m/LFC$  increase progressively, becoming close to or larger than unity in  
6  
7 565 correspondence to the initiation of intense precipitation. This confirms that the uplift forced by the  
8  
9 566 Alps is able to trigger convective activity, since the air parcels are forced to rise above the level of  
10  
11 567 free convection. Moreover, low CAPE values are consistent with the presence of weak to moderate  
12  
13 568 convection, acting to locally enhance rainfall rates. V2010, besides being the longest lasting event,  
14  
15 569 is also characterised by a more pronounced potential for convection development (Figure 11). It is  
16  
17 570 worth noting that rainfall enhancement over the windward slopes of the orography can be also due  
18  
19 571 to small-scale turbulence and microphysical processes (i.e. seeder-feeder mechanism), as described  
20  
21 572 for the western Alps for unblocked low-level flow (Rotunno and Houze, 2007).  
22  
23  
24  
25  
26

27 574 **4.5 Precipitation phase and the role of the cold pool in the Upstream events**

28  
29 575 When convection initiates resulting from uplift over the cold layer, the southerly low-level moist  
30  
31 576 flow is intercepted by the convergence line and hardly reaches the Alps. The convergence line  
32  
33 577 persists almost in the same position for several hours. Thus, although the direct orographic forcing  
34  
35 578 is not the main lifting mechanism, the Alps are responsible for the persisting blocked-flow  
36  
37 579 conditions, as displayed by the Fr analysis in Section 4.2. This can account for the stationarity of  
38  
39 580 the convective systems. However, the formation of evaporative cold pools is crucial in determining  
40  
41 581 organisation and propagation properties of convective systems (Emanuel, 1994). In the present  
42  
43 582 cases, cold-air layer formation precedes the convection onset; however, once convection has  
44  
45 583 developed, cold pools can be reinforced by evaporative cooling and can thus interact with the  
46  
47 584 upstream flow, forcing the low-level flow up and over its head (Bresson et al. 2012; Miglietta and  
48  
49 585 Rotunno 2009). In order to explore this aspect, additional MOLOCH simulations were performed  
50  
51 586 for the three Upstream events. These experiments were similar to their respective control runs,  
52  
53 587 except that the contribution to the temperature tendency due to evaporation or sublimation of  
54  
55 588 precipitation was removed in the microphysics parameterisation scheme.  
56  
57  
58  
59  
60

Figure 12 presents the results for M2007. The accumulated rainfall (Figure 12(a)) indicates that, in this simulation, the convective system persists over the plain of the Veneto region, just inland the Adriatic coast. With respect to the control simulation (Figure 4(e)), the precipitation maximum is shifted about 20 km to the northeast and displays a different orientation, although the intensity does not differ markedly (370 mm/12h). The lack of the precipitation band over the sea, parallel to the coast, reveals the main difference between the two simulations. The triggering phase is very similar, but during the mature stage the evaporative cooling actually reinforces the cold pool. Thus, in the control simulation (Figure 8(d)) the convective system slightly propagates against the low-level environmental flow blowing from the Adriatic Sea, as can be seen comparing Figures 8 (b) and (d). Conversely, without the cooling effect of the evaporation beneath the convective system, the low-level atmosphere upstream of the Alps is warmer and the signature of the cold pool much less evident (Figure 12 (b)). The convergence line, the convective updraft and hence the precipitation system remain over land, north of the coastline but still upstream of the orography.

It is worth mentioning that additional experiments were performed in order to evaluate the respective impact on the cooling of evaporation and sublimation of the precipitation. It turned out that the main contribution comes from rainfall evaporation, since the sublimation of ice microphysical hydrometeors does not change the results significantly, with respect to the control simulations.

Similar results were obtained for the other two events. Therefore, such experiments indicate that although evaporation/sublimation of precipitation is able to influence to some extent propagation and hence position of convection, it does not determine the stationarity of the systems. Upstream convergence due to persisting blocked-flow conditions is the primary mechanism producing that stationarity.

Following Miglietta and Rotunno (2009), the convective system is triggered and continuously regenerated as expected when  $h_m/LFC$  is larger than one (Table 3). Moreover, their idealised simulations of conditionally unstable flow past a mountain ridge showed that stationary convection

1  
2  
3 615 occurs when the advective time scale  $\tau_a$  is longer than the convective time scale  $\tau_c$ . Although the  
4  
5 616 applicability of theoretical results is not always straightforward for real events (Miglietta and  
6  
7 617 Rotunno 2012, Bresson et al. 2012) an estimation of the proposed non-dimensional parameters is  
8  
9 618 presented in the following. Table 3 lists the relevant parameters, evaluated for upstream conditions:  
10  
11 619 Downdraft Convective Available Potential Energy (DCAPE),  $CAPE^{1/2} / U$ , which is almost  
12  
13 620 proportional to  $\tau_a / \tau_c$ ,  $DCAPE^{1/2} / U$ , representing a measure of cold-pool propagation and  $N LFC /$   
14  
15 621  $U$ , which evaluates the impact of cold pool propagation on the upstream flow.  
16  
17 622 The results for M2007 and M2009 are very similar and the location of the precipitation seems to be  
18  
19 623 correlated with the theoretical results. Moderate wind speed and large instability (large values of  
20  
21 624  $CAPE^{1/2} / U$ ) are consistent with a stationary convective system upstream of the mountain ridge,  
22  
23 625 since there is enough time for evaporative reinforcement of the cold pool and redevelopment of  
24  
25 626 convective cells over the same area ( $\tau_a > \tau_c$ ). Moreover, the intensity of downdraft indicates the  
26  
27 627 possibility to have a slight propagation of the cold pool against the low-level environmental flow  
28  
29 628 for M2007, as actually observed. For IOP18 the comparison is even more difficult, since it is a low-  
30  
31 629 CAPE case with very strong wind. Although parameters suggest the triggering of convection, it  
32  
33 630 seems that intense wind speed does not create favourable conditions for long-lasting stationary  
34  
35 631 convection, as instead occurs during M2007 and M2009. It can be argued that in this case other  
36  
37 632 mechanisms could have contributed to the organisation of the convective system. In particular,  
38  
39 633 cyclonic mesoscale forcing could have played a role during the first part of the precipitation phase  
40  
41 634 by advecting convective cells from the Adriatic Sea towards the convergence line and later on  
42  
43 635 favouring the deflection of the low-level flow. The strong vertical shear characterised by a variation  
44  
45 636 of the along-ridge component of the flow could have also affected the convective system evolution  
46  
47 637 (Miglietta and Rotunno, 2014).  
48  
49  
50  
51  
52  
53  
54  
55  
56  
57  
58  
59  
60

639 **5. Conclusions**

1  
2  
3 640 The present study was motivated by observations made during the HyMeX-SOP1 campaign, which  
4  
5 641 documented two heavy-precipitation episodes (IOP18 and IOP19) characterised by similar synoptic  
6  
7 642 situations and initial mesoscale conditions of blocked-flow impinging on the Alpine barrier but with  
8  
9 643 a completely different dynamical evolution, leading to different precipitation patterns. During  
10  
11 644 IOP18, blocked-flow conditions persisted and the low-level south-easterly flow came from the  
12  
13 645 Adriatic Sea and was then deflected in front of the orography as a north-easterly barrier wind,  
14  
15 646 creating a convergence line upstream of the orography, where convection was triggered. Heavy  
16  
17 647 precipitation affected the plain area of NEI well upstream of the orography. Conversely, during  
18  
19 648 IOP19 the south-easterly flow was blocked by the Alps only in the initial phase, but then  
20  
21 649 progressively penetrated inland reaching the Alpine ridge, consistent with flow-over conditions.  
22  
23 650 This situation produced intense rainfall over the orography. This evidence prompted a survey and  
24  
25 651 an analysis of other similar cases, in order to identify common mechanisms leading to two different  
26  
27 652 precipitation patterns over NEI.  
28  
29  
30  
31 653 Notwithstanding the peculiar features and the complexity of each analysed event, the present study,  
32  
33 654 based on high-resolution NWP model simulations validated and supported by observations, shows  
34  
35 655 clearly that the two different rainfall patterns belong to two different “regimes” of precipitation  
36  
37 656 event that often affect the NEI area, as summarised in the schematic diagram of Figure 13. For all  
38  
39 657 the events, the low-level south-easterly flow (Sirocco wind) is initially blocked by the Alps and  
40  
41 658 deflected as an easterly/north-easterly barrier wind over the NEI plain. The presence of pre-existing  
42  
43 659 cold air over the NEI plain, resulting from nocturnal radiative cooling, enhances the low-level  
44  
45 660 blocking. As the synoptic disturbance progresses, the low-level wind intensifies and, depending on  
46  
47 661 the thermodynamic vertical profile of the impinging flow, convective activity may be triggered in  
48  
49 662 the initial phase. In the Upstream events (Figure 13(a)), convection initiates well upstream of the  
50  
51 663 orography where the incoming flow is forced to rise over the cold layer characterised by the barrier  
52  
53 664 wind. Blocked-flow conditions persist and the convergence line between the Sirocco wind and the  
54  
55 665 barrier wind triggers further convection. The cold pool is even reinforced by evaporative cooling of  
56  
57  
58  
59  
60

1  
2  
3 666 the convective precipitation, but specific model simulations have proved that the stationarity of the  
4  
5 667 convective system is determined by the persisting blocked-flow conditions by the Alps, confirmed  
6  
7 668 by low  $Fr$  values. The low-level flow from the Adriatic Sea is intercepted and thus it feeds the  
8  
9 669 convection and does not reach the orography. Therefore, precipitation affects the NEI plain or even  
10  
11 670 the coastal area, far upstream from the Alps.  
12  
13 671 In the Alpine events (Figure 13(b)) convection does not develop as a result of the forced uplift over  
14  
15 672 the cold air. Flow-over conditions progressively become established and the low-level flow coming  
16  
17 673 from the Adriatic Sea reaches the Alps, while the cold air ahead of the orography is removed. This  
18  
19 674 is also supported by progressively increasing values of  $Fr$ . The barrier wind disappears and the  
20  
21 675 orographically forced uplift of the impinging flow produces intense precipitation over the Alps.  
22  
23 676 Therefore, rainfall location turns out to be the consequence of different dynamical behaviour of the  
24  
25 677 flow impinging on the orography and its thermodynamics characteristics are critical for the  
26  
27 678 triggering of convective activity due to uplift over the barrier wind cold layer. If the profile is  
28  
29 679 unstable and the LFC is located at low altitude, this uplift is strong enough to trigger convection  
30  
31 680 over the plain upstream. Indices such as LI, CAPE, TLIFT and  $h_b/LFC$  proved able to take into  
32  
33 681 account the mechanisms responsible for the different phenomena observed during the triggering  
34  
35 682 phase.  
36  
37 683 The results obtained for the convective events are in agreement with theoretical studies of  
38  
39 684 conditionally unstable flow over orography. The value of  $h_m/LFC$  much greater than unity indicates  
40  
41 685 occurrence of convection upstream of the orography and the other parameters indicate an  
42  
43 686 environment favourable for cold-pool development and triggering of convective cells upstream of  
44  
45 687 the mountains. As observed during the M2007 and M2009 events, stationary deep convection  
46  
47 688 develops and persists on the same area as the convective cold-pool propagation is nearly balanced  
48  
49 689 by the environmental inflow. Only IOP18 does not fit completely with the theoretical results. Low-  
50  
51 690 CAPE values and strong wind speed make this case quite particular and it is difficult to refer it to  
52  
53 691 idealised simulations proposed in the literature. However, for all the three Upstream events the  
54  
55  
56  
57  
58  
59  
60

1  
2  
3 692 evaporative cooling beneath the precipitation system plays only a secondary role in determining the  
4  
5 693 characteristics of the convective system. Indeed, stationarity of the convergence line and of the  
6  
7 694 convection upstream of the Alps is mainly ascribable to the persistence of blocked-flow conditions.  
8  
9 695 For these events, convective outflow can only slightly modify rainfall position and intensity.  
10  
11 696 Finally,  $h_m/LFC$  is also computed for the Alpine events during the intense precipitation phase, when  
12  
13 697 the thermodynamic profile of the impinging flow becomes unstable. Here,  $h_m/LFC$  confirms the  
14  
15 698 possible development of convection, embedded in the orographic stratiform precipitation,  
16  
17 699 responsible for locally enhancing the rain rates.  
18  
19  
20 700 Several other aspects will be explored in future studies. The role of neighbouring mountain ranges  
21  
22 701 (Apennines and Dinaric Alps) will be investigated as well as the role of intense air-sea interactions  
23  
24 702 on water vapour budget and boundary layer characteristics. Moreover, the analysis of additional  
25  
26 703 heavy-precipitation events will possibly provide a more robust statistical support to these results.  
27  
28  
29  
30  
31  
32  
33

34 706 **Acknowledgements:** This work represents a contribution to the HyMeX program. This work was  
35  
36 707 supported by the Italian flagship project RITMARE. The authors are grateful to two anonymous  
37  
38 708 reviewers for their pertaining remarks and comments, which helped improve this manuscript. The  
39  
40 709 authors thank Dr. Anna Fornasiero for providing radar images during the early stages of the study,  
41  
42 710 and Dr. Mario Miglietta, Dr. Andrew Barrett and Dr Andrea Buzzi for fruitful discussions and  
43  
44 711 relevant suggestions. Thanks also to Nick Byrne for having carefully read the manuscript. The  
45  
46 712 authors wish to thank all the participants to the Italian national operational centre during the SOP1  
47  
48 713 field campaign: CNR (ISAC, IBIMET, IMAA), CETEMPS, Università La Sapienza, ISPRA,  
49  
50 714 Università Parthenope, OSMER-ARPA FVG, ARPA Piemonte, ARPAV, ARPA-SIMC, LaMMA,  
51  
52 715 ARPAL, Centro Funzionale Abruzzo, Centro Funzionale Marche, Centro Funzionale Umbria.  
53  
54 716 Thanks also to the National Department of Civil Protection (DPC) and to the CIMA foundation for  
55  
56 717 providing data of the national raingauge and radar network.  
57  
58  
59  
60



1  
2  
3  
4  
5  
6  
7  
8  
9  
10  
11  
12  
13  
14  
15  
16  
17  
18  
19  
20  
21  
22  
23  
24  
25  
26  
27  
28  
29  
30  
31  
32  
33  
34  
35  
36  
37  
38  
39  
40  
41  
42  
43  
44  
45  
46  
47  
48  
49  
50  
51  
52  
53  
54  
55  
56  
57  
58  
59  
60

718  
  
719  
  
720  
  
721  
  
722  
  
723  
  
724  
  
725  
  
726  
  
727  
  
728  
  
729  
  
730  
  
731  
  
732  
  
733  
  
734  
  
735  
  
736  
  
737  
  
738  
  
739  
  
740  
  
741  
  
742  
  
743

**REFERENCES**

Barbi A, Monai M, Racca R, Rossa AM. 2012. Recurring features of extreme autumnal rainfall events on the Veneto coastal area. *Nat. Hazards Earth Syst. Sci.* **12**: 2463-2477.

Barrett A, Gray S, Kirshbaum D, Nigel R, Schultz D, Fairman JG. 2014. Synoptic versus orographic control on stationary convective banding. *Q. J. R. Meteorol. Soc.* **141**: 1101-1113.

Billet S, Toro EF. 1997. On WAF-type schemes for multidimensional hyperbolic conservation laws. *J. Comput. Phys.* **130**: 1–24.

Borga M, Boscolo P, Zanon F, Sangati M. 2007. Hydrometeorological analysis of the 29 August 2003 flash flood in the Eastern Italian Alps. *J. Hydrometeorol.* **8**: 1049-1067.

Bougeault P, Binder P, Buzzi A, Dirks R, Kuettner J, Smith RB, Steinacker R, Volkert H. 2001. The MAP special observing period. *Bull. Amer. Meteorol. Soc.* **82**: 433-462.

Bousquet O, Smull BF. 2003. Observations and impacts of upstream blocking during a widespread orographic precipitation event. *Q. J. R. Meteorol. Soc.* **129**: 391-410.

Bresson R, Ricard D, Ducrocq V. 2009. Idealized mesoscale numerical study of Mediterranean heavy precipitating convective systems. *Meteorol. Atmos. Phys.* **103**: 45-55.

Bresson R, Ducrocq V, Nuissier O, Ricard D, de Saint-Aubin C. 2012. Idealized numerical simulations of quasi-stationary convective systems over the Northwestern Mediterranean complex terrain. *Q. J. R. Meteorol. Soc.* **138**: 1751-1763.

Buzzi A. 2004. Heavy precipitation and Alpine orography. In *Proceedings of the International Workshop on timely warnings of heavy precipitation episodes and flash floods*, Ljubljana, Slovenia, 12pp.

Buzzi A, Foschini L. 2000. Mesoscale meteorological features associated with heavy precipitation in the southern Alpine region. *Meteorol. Atmos. Phys.* **72**: 131-146.

Buzzi A, D'Isidoro M, Davolio S. 2003. A case study of an orographic cyclone south of the Alps during the MAP SOP. *Q. J. R. Meteorol. Soc.* **129**: 1795-1818.



- 744 Buzzi A, Davolio S, Malguzzi P, Drofa O, Mastrangelo D. 2014. Heavy rainfall episodes over  
745 Liguria of autumn 2011: numerical forecasting experiments. *Nat. Hazards Earth Syst. Sc.* **14**: 1325-  
746 1340.
- 747 Chen SH, Lin YL. 2005. Effects of moist Froude number and CAPE on a conditionally unstable  
748 flow over a mesoscale mountain ridge. *J. Atmos. Sci.* **62**: 331-350.
- 749 Davolio S, Buzzi A, Malguzzi P. 2009a. Orographic triggering of long-lived convection in three  
750 dimensions. *Meorol. Atmos. Phys.*, **103**, 35-44.
- 751 Davolio S, Mastrangelo D, Miglietta MM, Drofa O, Buzzi A, Malguzzi P. 2009b. High resolution  
752 simulations of a flash flood near Venice. *Nat. Hazards Earth Syst. Sci.* **9**: 1671-1678.
- 753 Davolio S, Miglietta MM, Diomede T, Marsigli C, Montani A. 2013. A flood episode in Northern  
754 Italy: multi-model and single-model mesoscale meteorological ensembles for hydrological  
755 predictions. *Hydrol. Earth Syst. Sci.* **17**: 1-14.
- 756 Davolio S, Ferretti R, Baldini L, Casaioli M, Cimini D, Ferrario ME, Gentile S, Loglisci N, Maiello  
757 I, Manzato A, Mariani S, Marsigli C, Marzano FS, Miglietta MM, Montani A, Panegrossi G, Pasi F,  
758 Pichelli E, Pucillo A, Zinzi A. 2015. The role of the Italian scientific community in the first HyMeX  
759 SOP: an outstanding multidisciplinary experience. *Meteorol. Zeit.*, doi:10.1127/metz/2015/0624.
- 760 Di Muzio E. 2014: Climatological characterization and dynamics of barrier winds in the Italian  
761 region. *PhD Thesis*, <http://amslaurea.unibo.it/6688> (accessed 02 October 2015).
- 762 Doswell CA, Ramis C, Romero R, Alonso S. 1998. A diagnostic study of three heavy precipitation  
763 episodes in the western Mediterranean. *Weather Forecasting.* **13**: 102-124.
- 764 Drobinski P, Ducrocq V, Alpert P, Anagnostou E, Béranger K, Borga M, Braud I, Chanzy A,  
765 Davolio S, Delrieu G, Estournel C, Filali Boubrahmi N, Font J, Grubisic V, Gualdi S, Homar V,  
766 Ivancan-Picek B, Kottmeier C, Kotroni V, Lagouvardos K, Lionello P, Llasat MC, Ludwig W,  
767 Lutoff C, Mariotti A, Richard E, Romero R, Rotunno R, Roussot O, Ruin I, Somot S, Taupier-  
768 Letage I, Tintore J, Uijlenhoet R, Wernli H. 2014. HyMeX, a 10-year multidisciplinary program on  
769 the Mediterranean water cycle. *Bull. Amer. Meteorol. Soc.* **95**: 1063-1082.

1  
2  
3 770 Drofa OV, Malguzzi P. 2004. Parameterization of microphysical processes in a non hydrostatic  
4  
5 771 prediction model. In *Proceedings of 14th International Conference on Clouds and Precipitation*,  
6  
7 772 Bologna, Italy, 1297-1300.  
8  
9  
10 773 Ducrocq V, Braud I, Davolio S, Ferretti R, Flamant C, Jansa A, Kalthoff N, Richard E, Taupier-  
11  
12 774 Letage I, Ayrat PA, Belamari S, Berne A, Borga M, Boudevillain B, Bock O, Boichard JL, Bouin  
13  
14 775 MN, Bousquet O, Bouvier C, Chiggiato J, Cimini D, Corsmeier U, Coppola L, Cocquerez P, Defer  
15  
16 776 E, Delanoë J, Di Girolamo P, Doerenbecher A, Drobinski P, Dufournet Y, Fourrié N, Gourley JJ,  
17  
18 777 Labatut L, Lambert D, Le Coz J, Marzano FS, Molinié G, Montani A, Nord G, Nuret M, Ramage  
19  
20 778 K, Rison B, Roussot O, Said F, Schwarzenboeck A, Testor P, Van Baelen J, Vincendon B, Aran M,  
21  
22 779 Tamayo J. 2014. HyMeX-SOP1, the field campaign dedicated to heavy precipitation and flash  
23  
24 780 flooding in the northwestern Mediterranean. *Bull. Amer. Meteorol. Soc.* **95**: 1083-1100.  
25  
26  
27 781 Emanuel K. A. 1994. *Atmospheric Convection*. Oxford University Press, 580 pp.  
28  
29 782 Ferretti R, Pichelli E, Gentile S, Maiello I, Cimini D, Davolio S, Miglietta MM, Panegrossi G,  
30  
31 783 Baldini L, Pasi F, Marzano FS, Zinzi A, Mariani S, Casaioli M, Bartolini G, Loglisci N, Montani A,  
32  
33 784 Marsigli C, Manzato A, Pucillo A, Ferrario ME, Colaiuda V, Rotunno R. 2014. Overview of the  
34  
35 785 first HyMeX Special Observation Period over Italy: observations and model results. *Hydrol. Earth*  
36  
37 786 *Syst. Sci.* **18**:1953-1977.  
38  
39  
40 787 Frei C, Schär C. 1998. A precipitation climatology of the Alps from high-resolution rain-gauge  
41  
42 788 observations. *Int. J. Climatol.* **18**: 873-900.  
43  
44  
45 789 Galway JG. 1956. The lifted index as a predictor of latent instability. *Bull. Amer. Meteorol. Soc.* **37**:  
46  
47 790 528-529.  
48  
49  
50 791 Isotta FA, Frei C, Weilguni V, Percec Tadic M, Lassegues P, Rudolf B, Pavan V, Cacciamani C,  
51  
52 792 Antolini G, Ratto SM, Munari M, Micheletti S, Bonati V, Lussana C, Ronchi C, Panettieri E,  
53  
54 793 Marigo G, Vertacnik G. 2013. The climate of daily precipitation in the Alps: development and  
55  
56 794 analysis of a high-resolution grid dataset from pan-Alpine rain-gauge data. *Int. J. Climatol.* **34**:  
57  
58 795 1657-1675.  
59  
60

- 796 Kain JS. 2004. The Kain-Fritsch convective parameterization: an update. *J. Appl. Meteorol.* **43**:  
797 170-181.
- 798 Lin YL, Reeves HD, Chien SY, Chiao S. 2005. Formation mechanisms for convection over  
799 Ligurian Sea during MAP IOP-8. *Mon. Weather Rev.* **133**: 2227-2245.
- 800 Malguzzi P, Grossi G, Buzzi A, Ranzi R, Buizza R. 2006. The 1966 'century' flood in Italy: A  
801 meteorological and hydrological revisitation. *J. Geophys. Res.* **111**: D24106,  
802 doi:10.1029/2006JD007111.
- 803 Manzato A. 2003. A climatology of instability indices derived from Friuli Venezia Giulia  
804 soundings, using three different methods. *Atmos. Res.* **67-68**: 417-454.
- 805 Manzato A. 2007. The 6 h climatology of thunderstorms and rainfalls in the Friuli Venezia Giulia  
806 plain. *Atmos. Res.* **83**: 336-348.
- 807 Manzato A, Davolio S, Miglietta MM, Pucillo A, Setvak M. 2015. 12 September 2012: A supercell  
808 outbreak in NE Italy? *Atmos. Res.* **153**: 98-118.
- 809 Manzato A, Cicogna A, Pucillo A. 2015. 6-hour maximum rain in Friuli Venezia Giulia:  
810 climatology and ECMWF-based forecasts. *Atmos. Res.* doi:10.1016/j.atmosres.2015.07.013 In  
811 press.
- 812 Massacand AC, Wernli H, Davies HC. 1998. Heavy precipitation on the Alpine southside: an  
813 upper-level precursor. *Geophys. Res. Lett.* **25**: 1435-1438.
- 814 Mazòn J, Pino D. 2013. The role of sea-land air thermal difference, shape of the coastline and sea  
815 surface temperature in the nocturnal offshore convection. *Tellus A* **65**: 1-13.
- 816 Miglietta MM, Buzzi A. 2004. A numerical study of moist stratified flow regimes over isolated  
817 topography. *Q. J. R. Meteorol. Soc.* **130**: 1749-1770.
- 818 Miglietta MM, Rotunno R. 2005. Simulations of moist nearly neutral flow over a ridge. *J. Atmos.*  
819 *Sci.* **62**: 1410-1427.
- 820 Miglietta MM, Rotunno R. 2009. Numerical simulations of conditionally unstable flows over a  
821 ridge. *J. Atmos. Sci.* **66**: 1865-1885.

1  
2  
3 822 Miglietta MM, Rotunno R. 2010. Numerical simulations of low-CAPE flows over a mountain  
4  
5 823 ridge. *J. Atmos. Sci.* **67**: 2391-2401.  
6  
7 824 Miglietta MM, Rotunno R. 2014. Numerical simulations of sheared conditionally unstable flows  
8  
9 825 over a mountain ridge. *J. Atmos. Sci.* **71**: 1747-1762.  
10  
11 826 Morcrette JJ, Barker HW, Cole JNS, Iacono MJ, Pincus R. 2008. Impact of a new radiation  
12  
13 827 package, McRad, in the ECMWF Integrated Forecasting System. *Mon. Weather. Rev.* **136**: 4773-  
14  
15 828 4798.  
16  
17 829 Monai M, Rossa AM, Bonan C. 2006. Partitioning of snowy and rainy precipitation in a case of a  
18  
19 830 north Adriatic frontal passage. *Advances in Geosciences* **7**: 279-284.  
20  
21 831 Nuissier O, Ducrocq V, Ricard D, Lebeaupin C, Anquetin S. 2008. A numerical study of three  
22  
23 832 catastrophic precipitating events over southern France. I: Numerical framework and synoptic  
24  
25 833 ingredients. *Q. J. R. Meteorol. Soc.* **134**: 111-130.  
26  
27 834 Pierrehumbert RT, Wyman B. 1985. Upstream effects of mesoscale mountains. *J. Atmos. Sci.* **42**:  
28  
29 835 977-1003.  
30  
31 836 Ricard D, Ducrocq V, Auger L. 2012. A climatology of the mesoscale environment associated with  
32  
33 837 heavily precipitating events over a northwestern Mediterranean area. *J. Appl. Meteorol. Climatol.*  
34  
35 838 **51**: 468-488.  
36  
37 839 Rudari R, Entekhabi D, Roth G. 2004. Terrain and multiple-scale interactions as factors in  
38  
39 840 generating extreme precipitation events. *J. Hydrometeorol.* **5**, 390-404.  
40  
41 841 Ritter B, Geleyn JF. 1992. A comprehensive radiation scheme for numerical weather prediction  
42  
43 842 models with potential applications in climate simulations. *Mon. Weather. Rev.* **120**: 303-325.  
44  
45 843 Rossa AM, Cenon G, Monai M. 2010. Quantitative comparison of radar QPE to rain gauges for  
46  
47 844 the 26 September 2007 Venice Mestre flood. *Nat. Hazards Earth Syst. Sci.* **10**: 371-377.  
48  
49 845 Rotach MW, Ambrosetti P, Ament F, Appenzeller C, Arpagaus M, Bauer HS, Behrendt A, Bouttier  
50  
51 846 F, Buzzi A, Corazza M, Davolio S, Denhard M, Dorninger M, Fontannaz L, Frick J, Fundel F,  
52  
53 847 Germann U, Gorgas T, Hegg C, Hering A, Keil C, Liniger MA, Marsigli C, McTaggart-Cowan R,  
54  
55  
56  
57  
58  
59  
60

- 848 Montani A, Mylne K, Ranzi R, Richard E, Rossa A, Santos-Muñoz D, Schär C, Seity Y, Staudinger  
849 M, Stoll M, Volkert H, Walser A, Wang Y, Werhahn J, Wulfmeyer V, Zappa M. 2009. MAP D-  
850 PHASE: Real-time Demonstration of Weather Forecast Quality in the Alpine Region. *Bull. Amer.*  
851 *Meteorol. Soc.* **90**: 1321-1336.
- 852 Rotunno R, Ferretti R. 2001. Mechanisms of intense Alpine rainfall. *J. Atmos. Sci.* **58**: 1732-1749.
- 853 Rotunno R, Ferretti R. 2003. Orographic effects on rainfall in MAP cases IOP2b and IOP8. *Q. J. R.*  
854 *Meteorol. Soc.* **129**: 373-390.
- 855 Rotunno R, Houze RA. 2007. Lessons on orographic precipitation from the Mesoscale Alpine  
856 Programme. *Q. J. R. Meteorol. Soc.* **133**: 811-830.
- 857 Schwerdtfeger W. 1984. Weather and Climate of the Antarctic. Elsevier Sciences Publisher, 261 pp.
- 858 Smith RB. 1979. The influence of mountains on the atmosphere. *Advances in Geophysics* **21**: 87-  
859 230.
- 860 Setvák M, Bedka K, Lindsey DT, Sokol A, Charvát Z, Štáštka J, Wang PK. 2013. A-Train  
861 observations of deep convective storm tops. *Atmos. Res.* **123**: 229-248.
- 862 Smolarkiewicz PK, Rotunno R. 1990. Low Froude number flow past three-dimensional obstacles.  
863 Part II: Upwind flow reversal zone. *J. Atmos. Sci.* **47**: 1498-1511.
- 864 Zampieri M, Malguzzi P, Buzzi A. 2005. Sensitivity of quantitative precipitation forecasts to  
865 boundary layer parameterization: a flash flood case study in the Western Mediterranean. *Nat.*  
866 *Hazards Earth Syst. Sci.* **5**: 603-612.
- 867

Event name (Acronym) Type of event	Initial Condition for BOLAM	Initial Condition for MOLOCH	Max Rainfall Observation (Simulation) Accumulation period
HyMeX - IOP19 (IOP19) Alpine	04 November 2012 00 UTC	04 November 2012 03 UTC	370 (350) mm/30h 04 Nov, 06 UTC – 05 Nov. 12 UTC
Piancavallo 2012 (P2012) Alpine	10 November 2012 12 UTC	10 November 2012 15 UTC	390 (310) mm/24h 11 Nov, 00 UTC – 12 Nov, 00 UTC
Vicenza 2010 (V2010) Alpine	30 October 2010 18 UTC	30 October 2010 21 UTC	600 (600) mm/48h 31 Oct, 00 UTC – 02 Nov, 00 UTC
HyMeX - IOP18 (IOP18) Upstream	31 October 2012 00 UTC	31 October 2012 06 UTC	120 (140) mm/24h 31 Oct, 12 UTC – 01 Nov, 12 UTC
Marghera 2007 (M2007) Upstream	25 September 2007 12 UTC	25 September 2007 18 UTC	320 (330) mm/12h 26 Sep. 00 UTC – 26 Sep. 12 UTC
Mira 2009 (M2009) Upstream	15 September 2009 18 UTC	16 September 2009 00 UTC	180 (210) mm/24h 16 Sep 00 UTC – 17 Sep 00 UTC

Table 1: List of analysed events and their acronyms, initialization time for BOLAM and MOLOCH simulations, accumulated (observed and forecast) precipitation and selected rainfall accumulation period.

876

Alpine event	Analysed time	Initiation of intense precipitation	CAPE ( $\text{J kg}^{-1}$ )	Lifted Index (K)	$h_b$ (m)	U ( $\text{m s}^{-1}$ )
IOP19	04 Nov 2012 15 UTC	04 Nov 2012 18 UTC	100	2.2	480	13.2
P2012	10 Nov 2012 18 UTC	11 Nov 2012 00 UTC	3	4.6	500	12.3
V2010	31 Oct 2010 03 UTC	31 Oct 2010 06 UTC	40	4.3	480	12.1

877

878 Table 2: Summary of parameters computed for the triggering phase for the three Alpine events.

879 Convective Available Potential Energy (CAPE), Lifted Index (LI), depth of the stable layer

880 characterised by barrier wind over the NEI plain ( $h_b$ ), meridional component of the wind averaged

881 among the model levels below 2000 m (U). The most unstable parcel was used in the computation.

882

Upstream event	Analysed time	Initiation of intense precipitation	CAPE (J kg <sup>-1</sup> )	Lifted Index (K)	LFC (m)	h <sub>b</sub> (m)	h <sub>b</sub> /LFC	h <sub>m</sub> /LFC	U (m s <sup>-1</sup> )	DCAPE (J kg <sup>-1</sup> )	CAPE <sup>1/2</sup> /U	DCAPE <sup>1/2</sup> /U	N LFC/U
IOP18	31 Oct 2012 20 UTC	31 Oct 2012 22 UTC	190	0.5	340	780	2.3	5.9	22.8	120	0.6	0.5	0.15
M2007	26 Sep 2007 03 UTC	26 Sep 2007 05 UTC	1190	-3.9	480	480	1.0	4.2	7.4	680	4.7	3.5	0.52
M2009	16 Sep 2007 07 UTC	16 Sep 2009 10 UTC	2060	-5.3	480	600	1.3	4.2	12.4	450	3.7	1.7	0.33

Table 3: Summary of parameters computed for the triggering phase for the three Upstream events. Convective Available Potential Energy (CAPE), Lifted Index (LI), depth of the stable layer characterised by barrier wind over the NEI plain (h<sub>b</sub>), ratio between h<sub>b</sub> and LFC, ratio between ridge height (h<sub>m</sub> = 2000 m) and LFC, meridional component of the wind averaged among the model levels below 2000 m (U), Downdraft Convective Available Potential Energy (DCAPE), CAPE<sup>1/2</sup>/U, DCAPE<sup>1/2</sup>/U, N LFC / U. The most unstable parcel was used in the computation.



## FIGURE CAPTIONS

Figure 1: area of interest corresponding to the MOLOCH integration domain and indication of the locations mentioned in the text: Venice (cross), Vicenza (plus), Padua (star), Concordia Sagittaria (dot) SODAR and Campoformido (Udine) sounding (triangle). The NEI area including the Friuli Venezia Giulia (FVG) and Veneto regions is also indicated. Model orography above 1500 meters is shaded.

Figure 2: synoptic situation for the six events (IFS - ECMWF analyses). Geopotential height at 500 hPa (dam, black lines), sea level pressure (hPa, white lines) and temperature at 500 hPa (°C, colour shading). (a) IOP19, 05 Nov. 2012 at 0600 UTC; (b) Piancavallo event, 11 Nov. 2012 at 0600 UTC; (c) Vicenza event, 01 Nov. 2010 at 0000 UTC; (d) IOP18, 31 Oct. 2012 at 1200 UTC; (e) Marghera event, 26 Sep. 2007 at 0600 UTC; (f) Mira event, 16 Sep. 2009 at 1200 UTC.

Figure 3: observed precipitation, obtained by interpolation of data provided by the dense networks of Veneto (about 170 rain-gauges) and FVG (about 260 rain-gauges) regional meteorological agencies, for the six events. (a) IOP19, 30-h accumulated precipitation at 1200 UTC, 05 Nov. 2012; (b) Piancavallo event, 24-h accumulated precipitation at 0000 UTC, 12 Nov. 2012; (c) Vicenza event, 48-h accumulated precipitation at 0000 UTC, 02 Nov. 2010; (d) IOP18, 24-h accumulated precipitation at 1200 UTC, 01 Nov. 2012; (e) Marghera event, 12-h accumulated precipitation at 1200 UTC, 26 Sep. 2007; (f) Mira event, 24-h accumulated precipitation at 0000 UTC, 17 Sep. 2009. The regional border of Veneto and FVG regions are also plotted.

Figure 4: as in Fig. 3, but for MOLOCH forecasts.

1  
2  
3 918 Figure 5: (a) High-resolution SODAR wind data in Concordia Sagittaria between 0300 and 1200  
4  
5 919 UTC, 31 Oct. 2010 (V2010 event). (b) High-resolution SODAR wind data in Padua between 0000  
6  
7 920 and 1200 UTC, 26 Sep. 2007 (M2007 event). Note that the time reported on the x-axis are in CET,  
8  
9 921 corresponding to UTC+1.  
10  
11 922  
12  
13  
14 923 Figure 6: evolution of the Froude number for the six heavy-precipitation events over the Alps,  
15  
16 924 Hours on x-axis are referred to the initiation of intense precipitation. Dashed (solid) lines for the  
17  
18 925 Upstream (Alpine) events.  
19  
20 926  
21  
22  
23 927 Figure 7: MOLOCH 10-meter wind ( $\text{m s}^{-1}$ , shading) during the initial stage of the events, when the  
24  
25 928 Sirocco wind is blocked by the orography and deflected as barrier wind ahead of the Alps: (a)  
26  
27 929 Vicenza event, 31 Oct. 2010, 0300 UTC; (b) Marghera event, 26 Sep. 2007, 0400 UTC. The black  
28  
29 930 dashed lines indicate the location of the vertical cross-sections shown in Fig. 8. The black square  
30  
31 931 indicates the area where averaged vertical profiles are computed. During the precipitation stage of  
32  
33 932 the events: (c) flow-over condition for the Vicenza event, 31 Oct. 2010, 1800 UTC; (d) persisting  
34  
35 933 blocked-flow condition for the Marghera event, 26 Sep. 2007, 1200 UTC. Note that only a portion  
36  
37 934 of the MOLOCH integration domain is shown. Black contours show the 500 m and 1500 m  
38  
39 935 orography elevation.  
40  
41  
42  
43 936  
44  
45 937 Figure 8: MOLOCH vertical cross-sections along the black line indicated in Fig. 7. Equivalent  
46  
47 938 potential temperature (thin contour line and colour shading, interval 2 K), tangent wind component  
48  
49 939 (vectors) and cloud water and ice (thick contour indicating  $0.1 \text{ g kg}^{-1}$ ), for Vicenza event (cross  
50  
51 940 section length 314 km), (a) 31 Oct. 2010, 0300 UTC and (c) 01 Nov. 2010, 1000 UTC; Marghera  
52  
53 941 event (cross section length 363 km), 26 Sep. 2007, (b) at 0400 UTC and (d) at 1200 UTC.  
54  
55  
56 942  
57  
58  
59  
60

Figure 9: vertical thermodynamic profiles simulated by MOLOCH during the initial stage of the events and computed as an average over an area of about 15 x 15 km for (a) Vicenza event, 31 Oct. 2010, 0300 UTC, in 45.1 °N, 12.9 °E; (b) Marghera event, 26 Sep. 2007, 0400 UTC, in 45 °N, 13 °E.

Figure 10: profiles of buoyancy for air parcels raised to a height of 500 m above their initial position (vertical axis). Profiles are computed for the initial stage of the events, before intense precipitation occurrence. Dashed (solid) lines for the Upstream (Alpine) events. Values on the x-axis are multiplied by  $10^2$ .

Figure 11: evolution of  $h_m/LFC$  for the three Alpine events. Hours on x-axis are referred to the initiation of intense precipitation.

Figure 12: results of MOLOCH simulations performed removing the contribution of evaporation/sublimation of the precipitation (see text). Marghera event (cross section length 363 km): (a) 12-h accumulated precipitation at 1200 UTC, 26 Sep. 2007; (b) vertical cross-sections along the black line of Fig. 7 showing equivalent potential temperature (thin contour line and colour shading, interval 2 K), tangent wind component (vectors) and cloud water and ice (thick contour indicating  $0.1 \text{ g kg}^{-1}$ ) on 26 Sep. 2007 at 1200 UTC.

Figure 13: schematic diagram of the key mechanisms responsible for the two different precipitation patterns over NEI. (a) Upstream event: blocked low-level flow, barrier wind, convergence and deep convection development occurring over the plain, upstream of the orography. (b) Alpine event: unblocked low-level flow, flow-over conditions, orographic lifting and precipitation over the Alps with possible embedded convection.

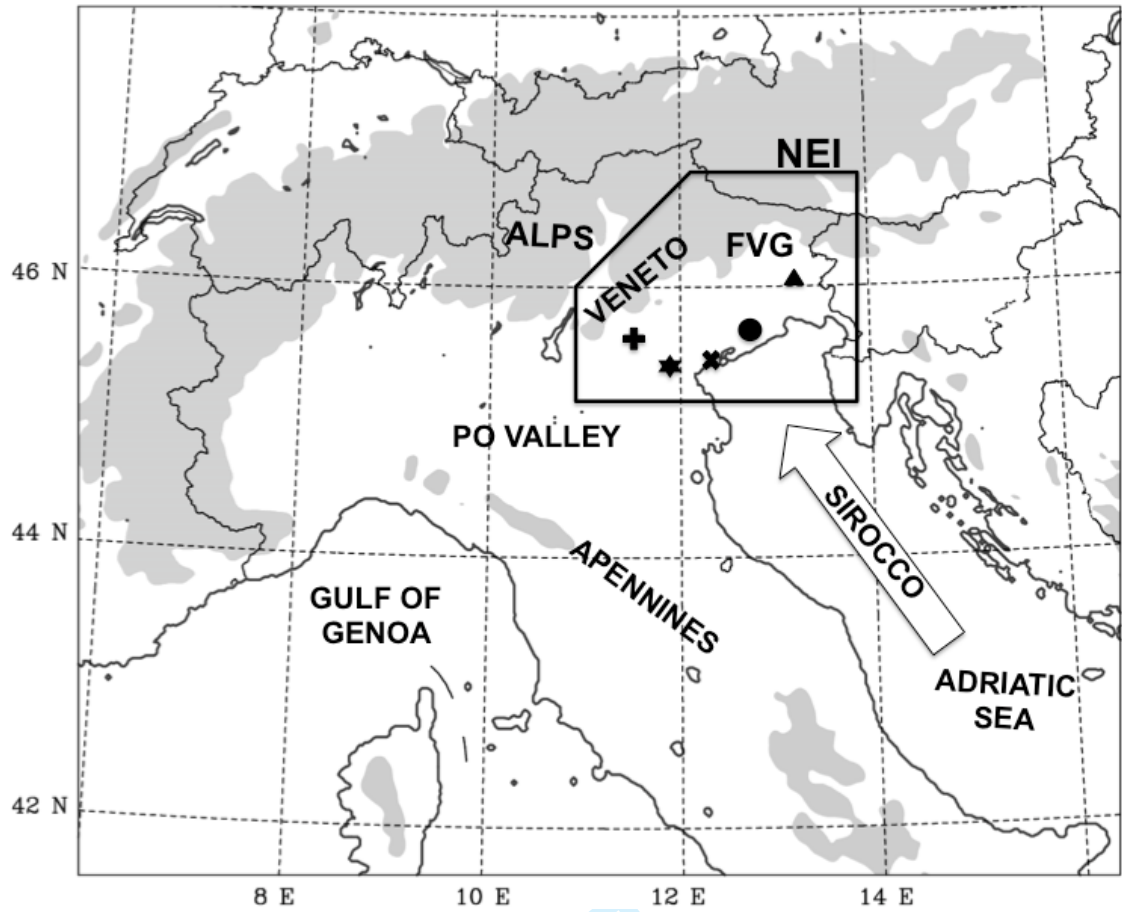


Figure 1

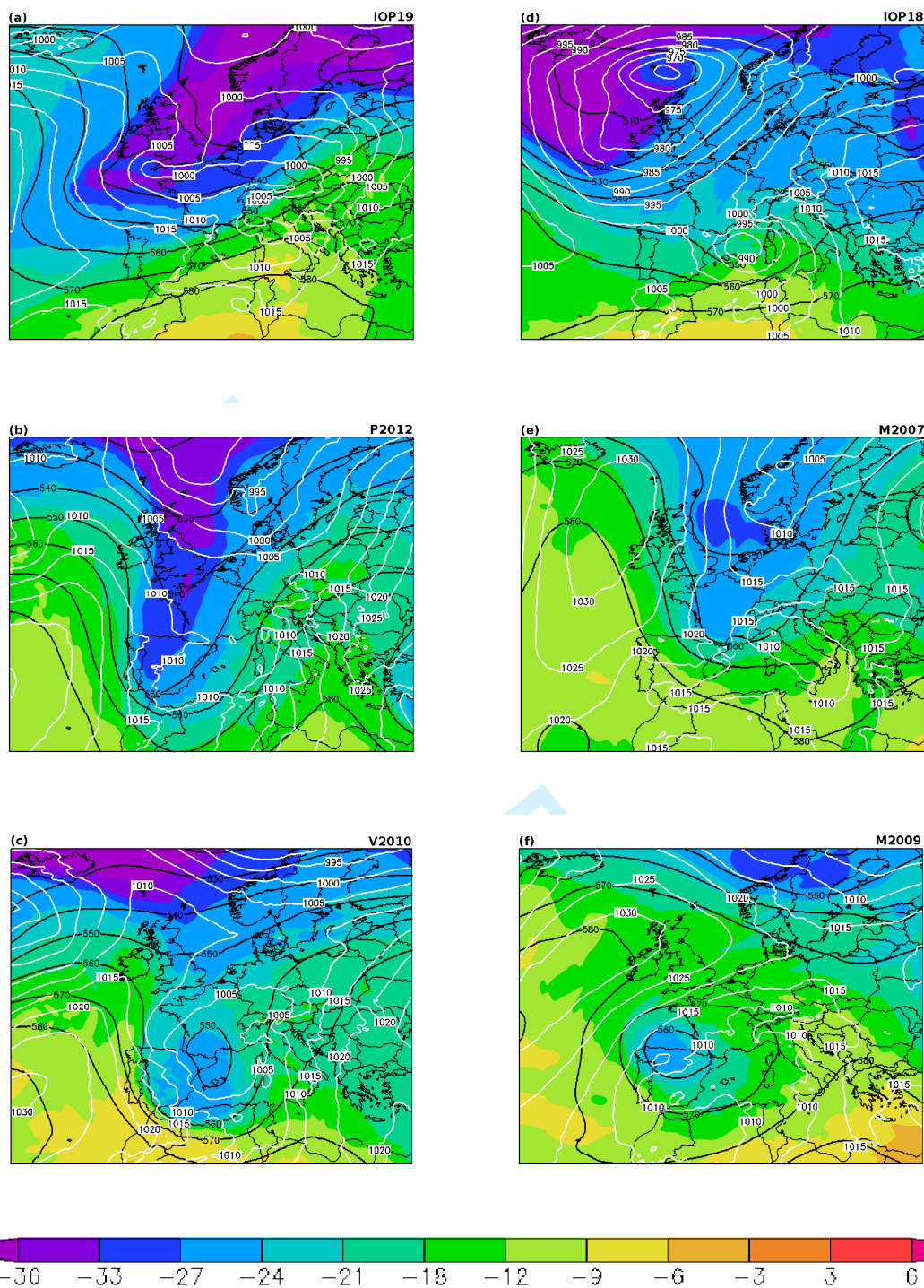


Figure 2



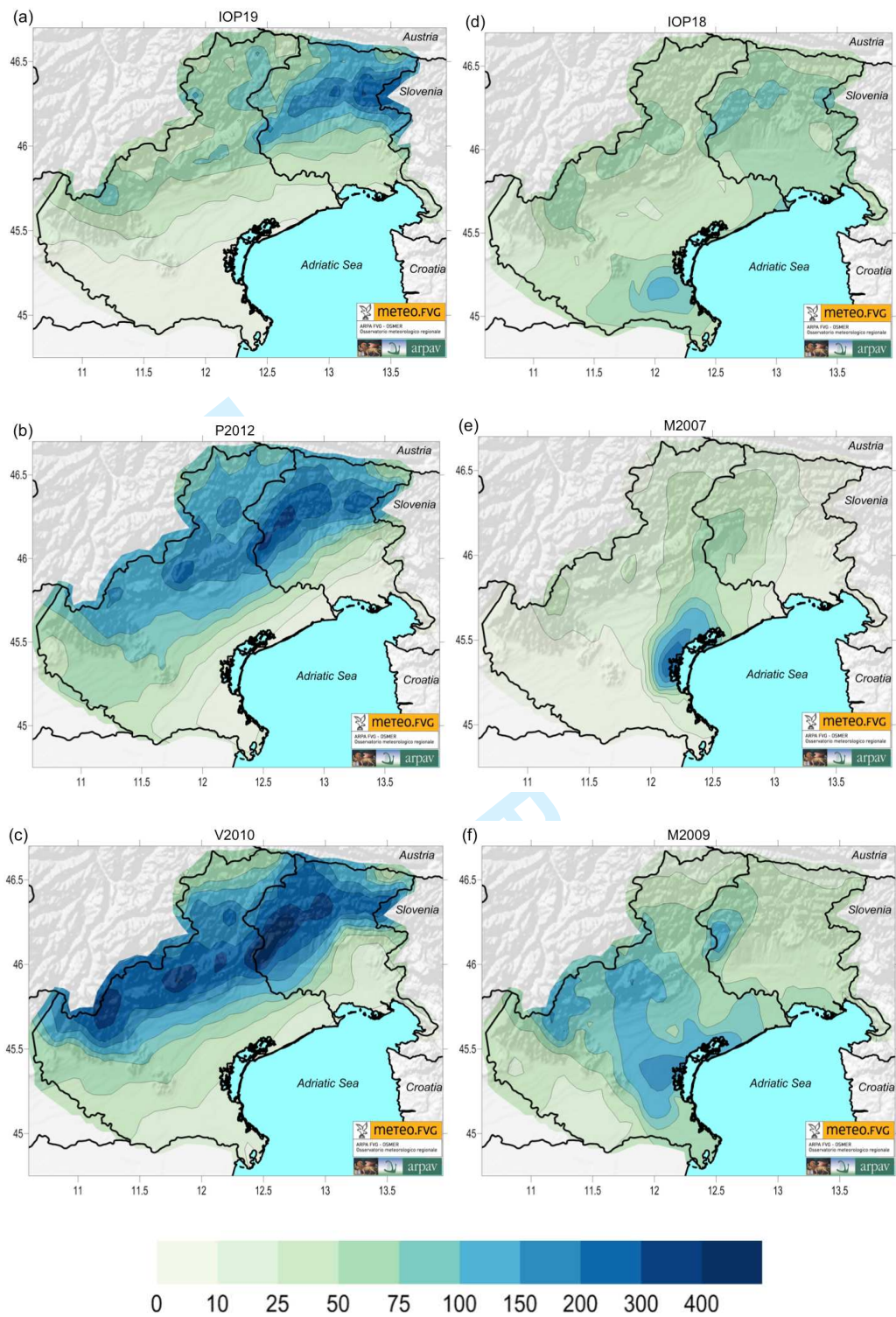


Figure 3

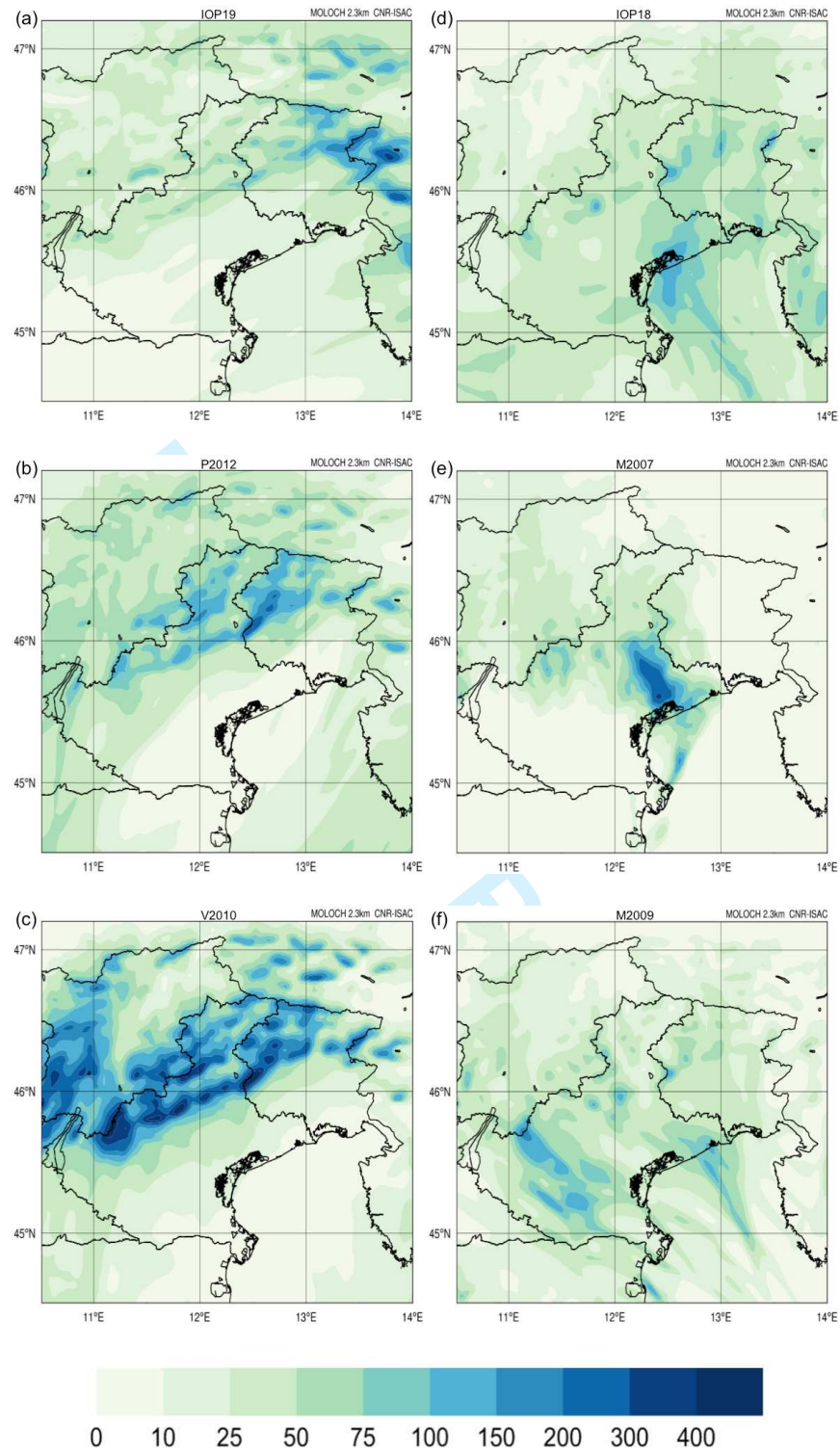


Figure 4



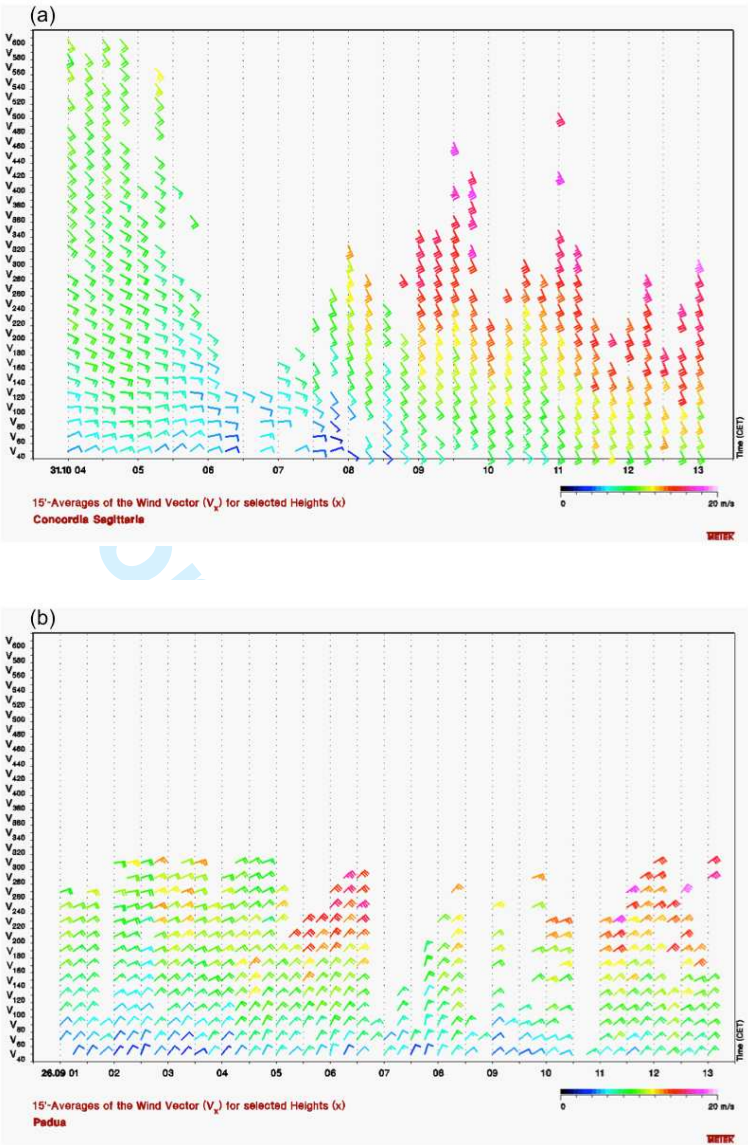


Figure 5

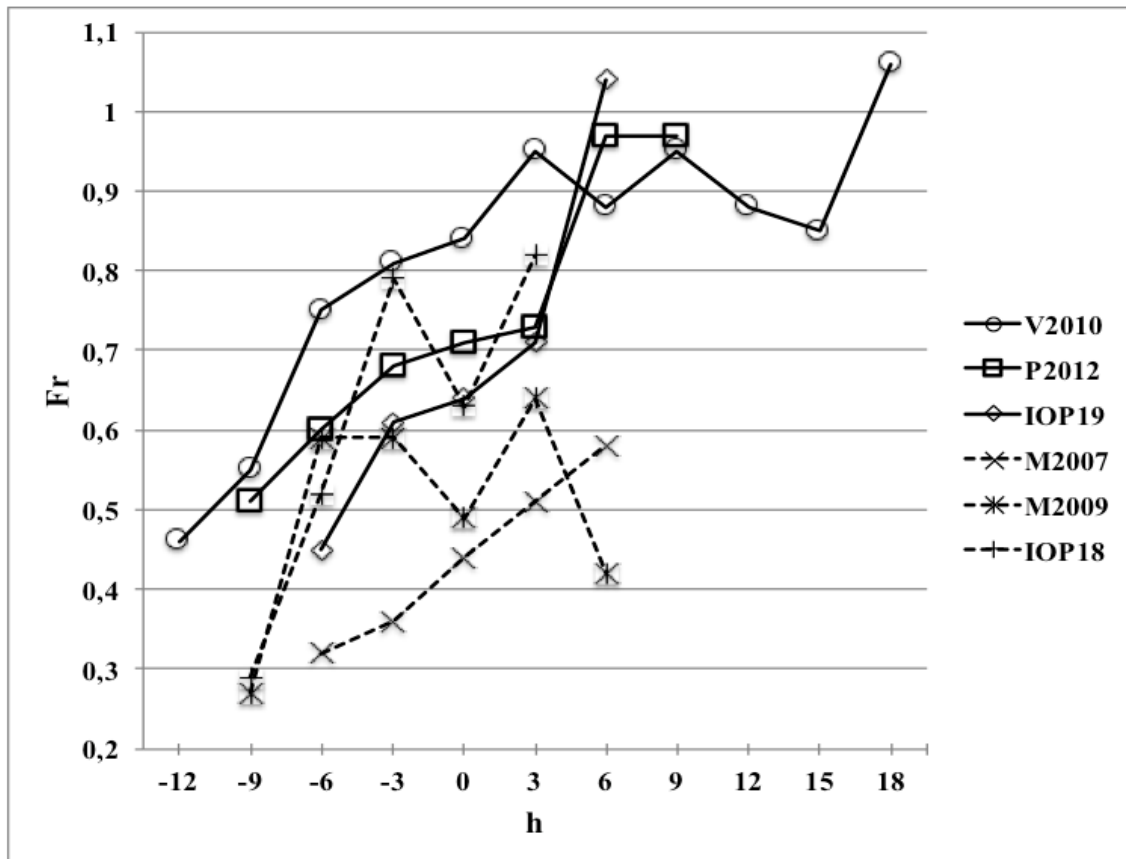


Figure 6

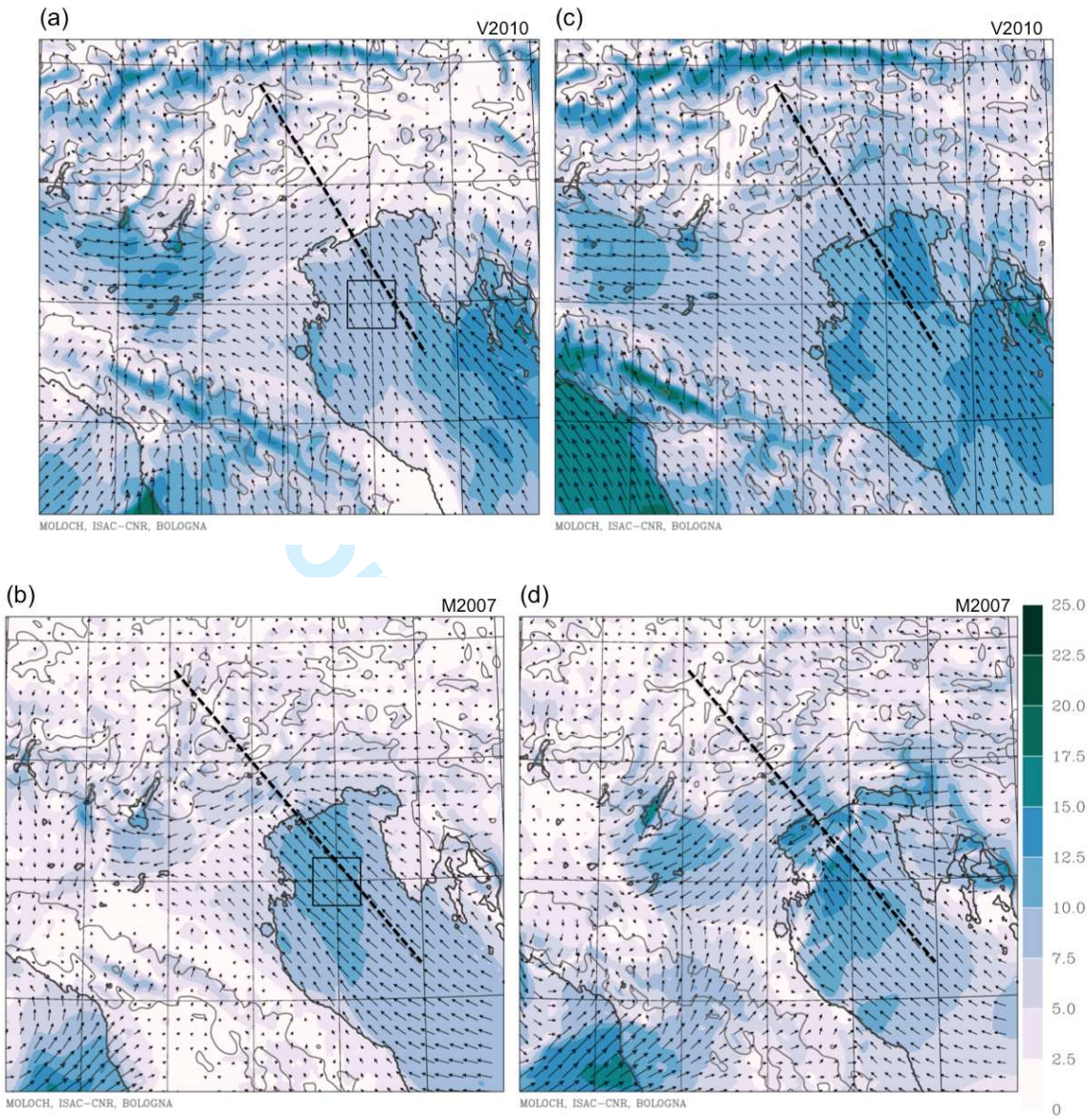


Figure 7



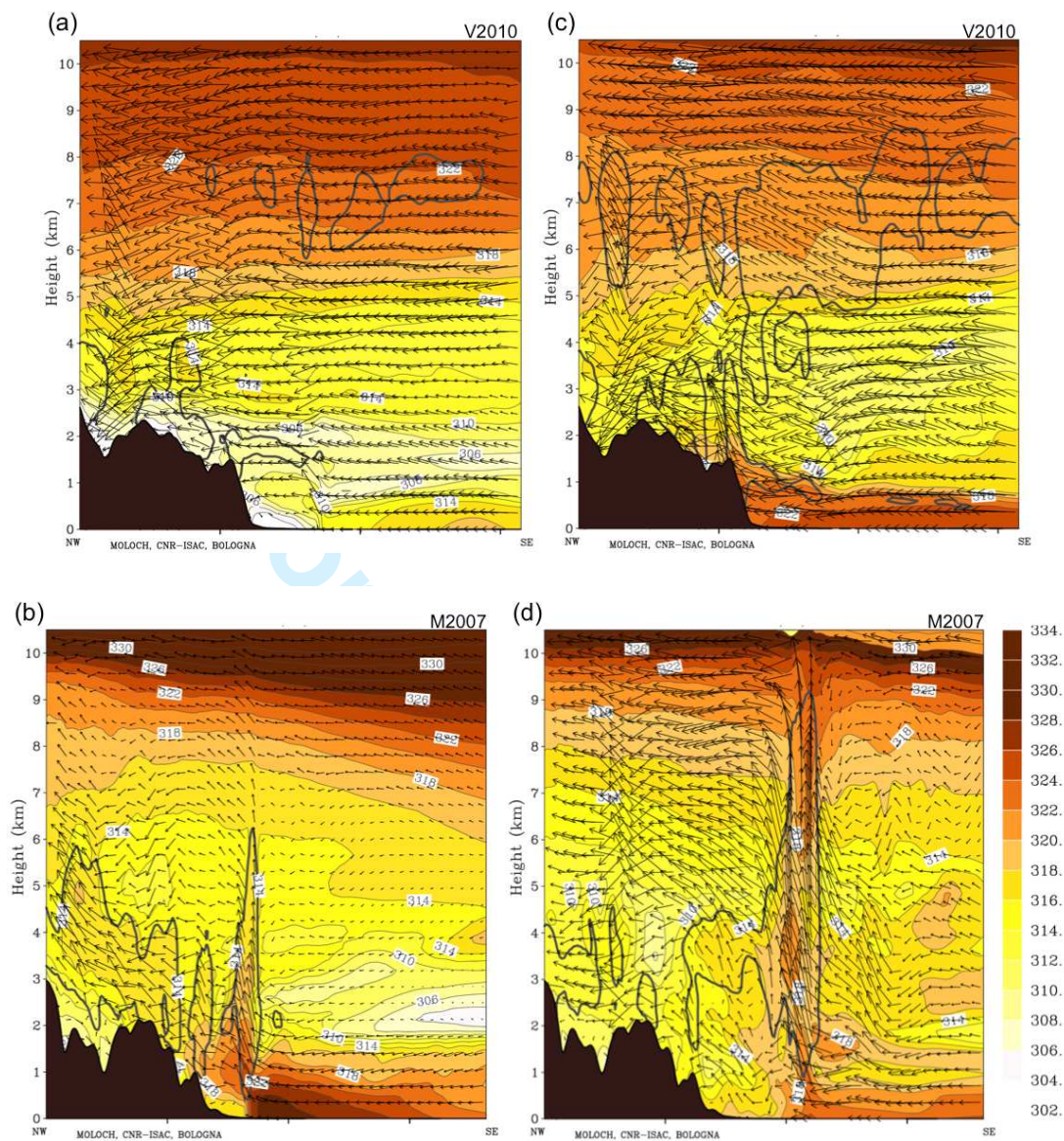


Figure 8

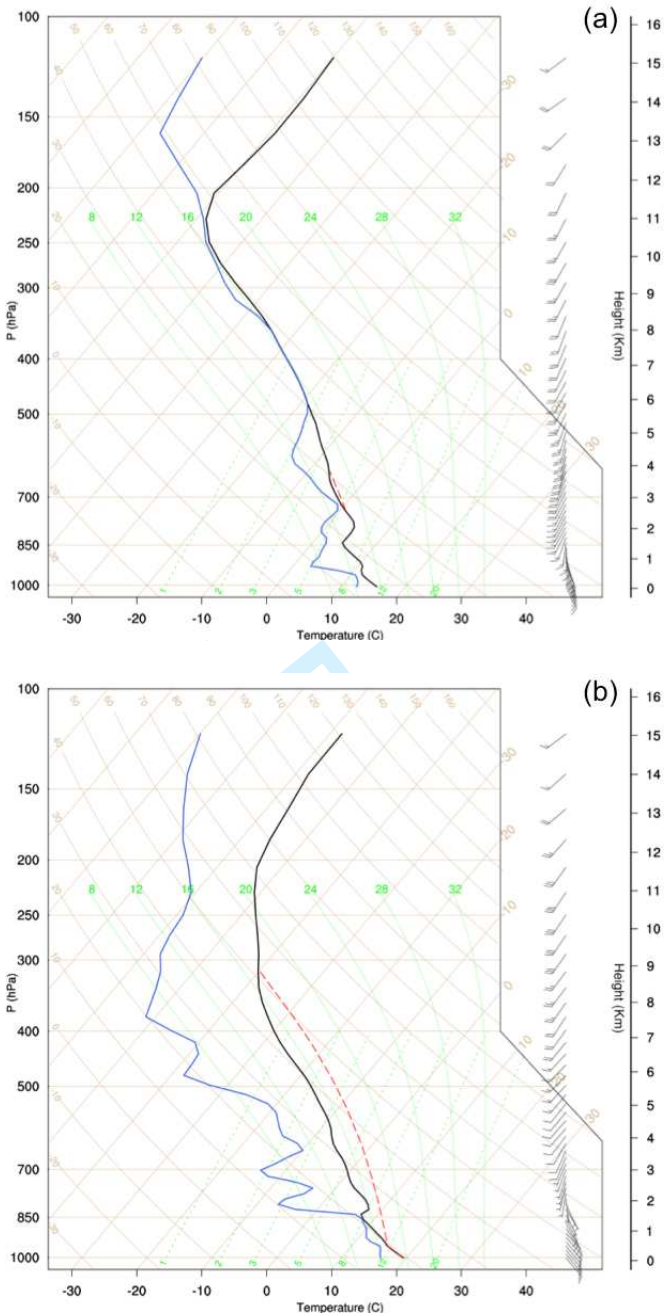


Figure 9

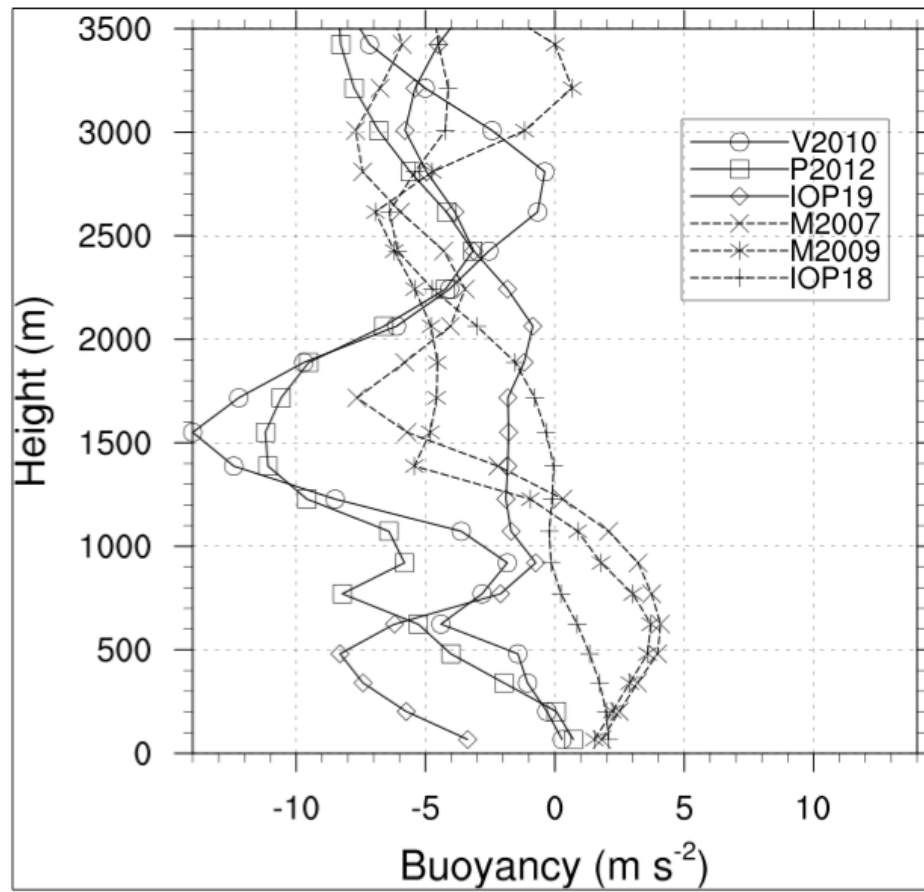


Figure 10

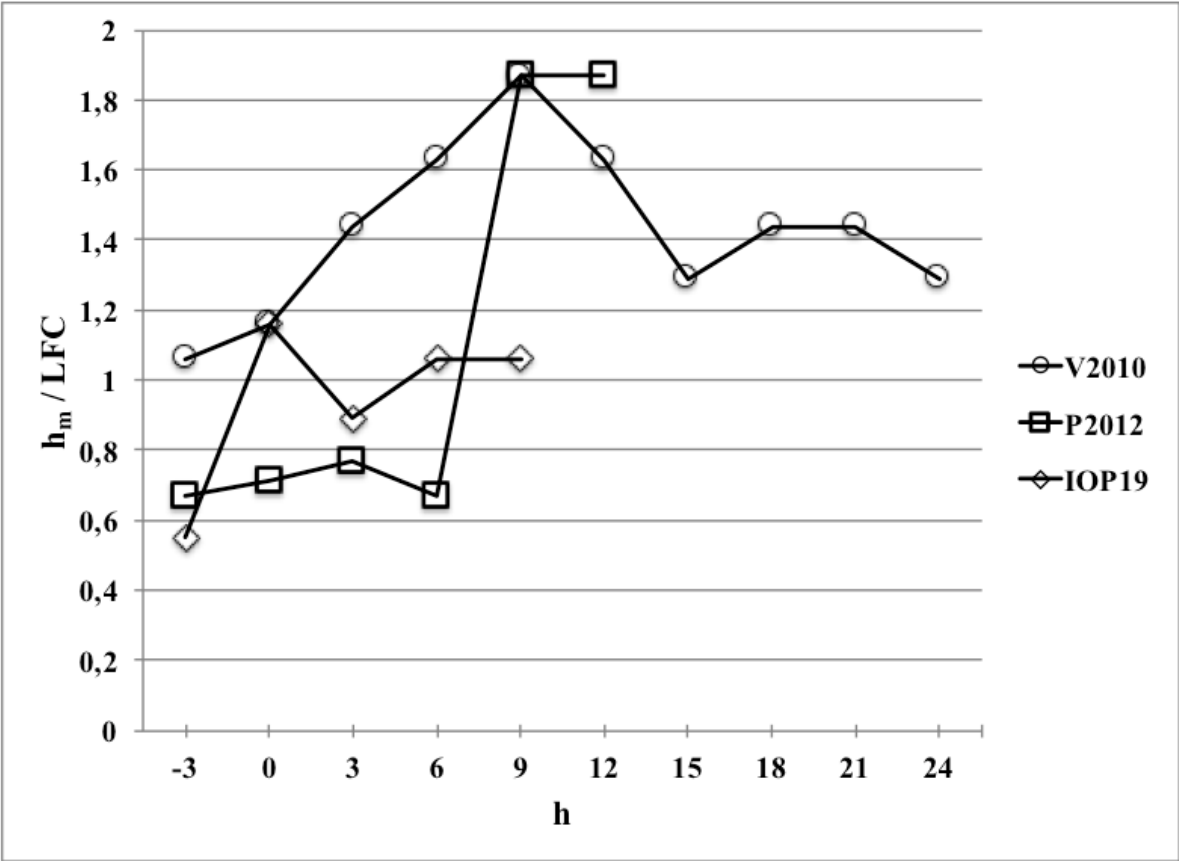


Figure 11



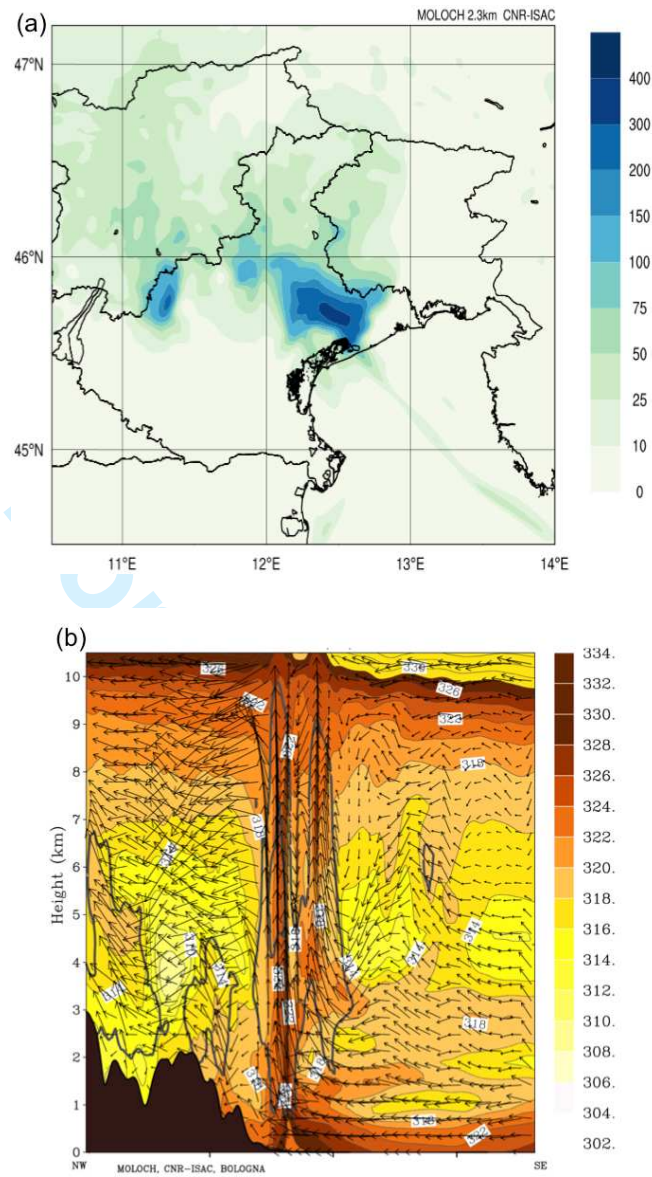


Figure 12

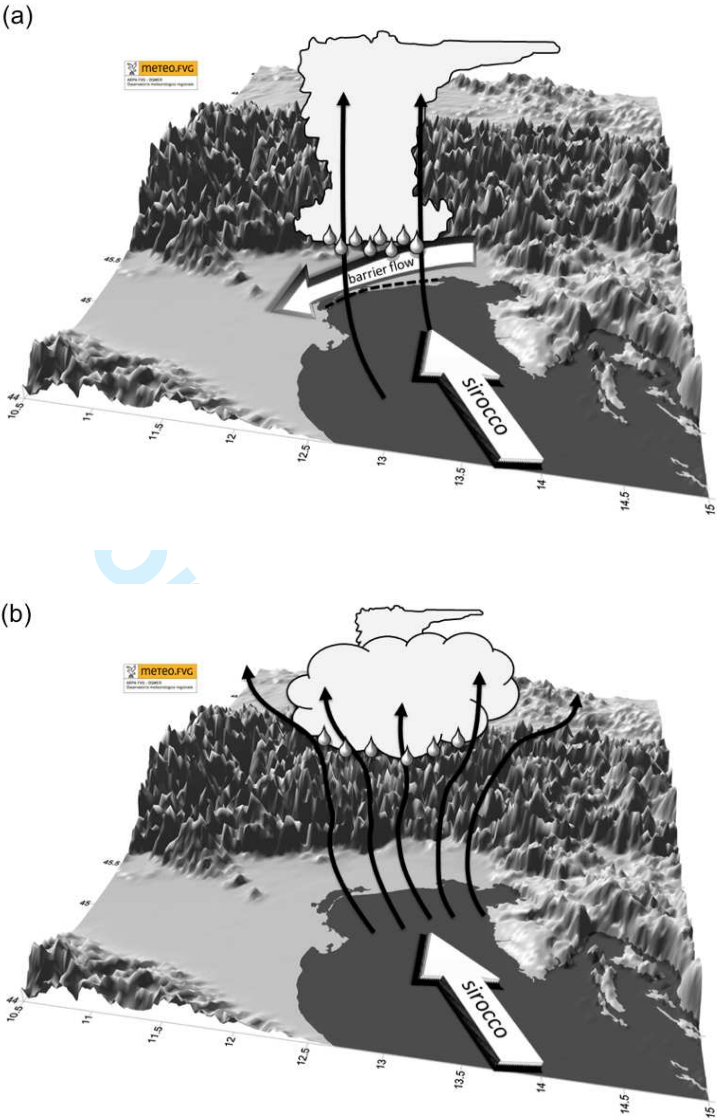


Figure 13